MAKERERE UNIVERSITY

INVESTIGATING THE INFLUENCE OF MASONRY INFILL WALLS ON THE SEISMIC RESPONSE OF REINFORCED CONCRETE FRAME STRUCTURES IN UGANDA

BY

KAKURU VERNY BAGUMA

BSC CIVIL ENGINEERING (MAK)

Signature:.....

Date:....14/05/2026.....

SUPERVISORS

DR. MOSES MATOVU

Signature: .....

Date:.....14|05|26.....

DR. ALLAN OKODI

Signature:.....Alokodi.....

Date:.....May 13, 2026.....

MAY 2026

DECLARATION

This original research study has been submitted to the Directorate of Research & Graduate Training in partial fulfilment of the requirements for the Master of Science in Civil Engineering degree at Makerere University. It is independent work that has not been submitted for any other degree at any other university.

.....

KAKURU VERNY BAGUMA

REG NO: 2023/HD08/2661U

This research has been submitted for examination with the approval of the following Supervisors

DR. MATOVU MOSES

Department of Civil & Environmental Engineering

College of Engineering, Design, Art, and Technology

Makerere University

Kampala – UGANDA

Signature: ..... **Date:** 14/05/2026

DR. ALLAN OKODI

Department of Civil & Environmental Engineering

College of Engineering, Design, Art, and Technology

Makerere University

Kampala – UGANDA

Signature: Alokodi **Date:** May 13, 2026

ABSTRACT

This study investigates the influence of masonry infill walls on the seismic response of Reinforced Concrete frame structures in Uganda, where current seismic design codes lack explicit provisions for infill wall and RC frame interactions. The study develops a site-specific design response spectrum for Uganda's highest seismic zone. Finite element modelling in ABAQUS was employed to simulate the detailed nonlinear in-plane behaviour of infilled and bare RC frames. For broader parametric studies across varying building heights and infill types, like, clay bricks and solid concrete blocks, the equivalent diagonal strut method was implemented in ETABS. Model validation was conducted against established experimental results from pseudo-dynamic tests, ensuring accuracy in displacement, drift, and base shear predictions. Nonlinear static pushover analyses were performed to evaluate seismic performance indicators, including lateral displacement, storey drift, base shear capacity, and stiffness contribution.

Results indicate that concrete block infills, owing to their higher compressive strength, provide greater initial stiffness and higher base shear capacity than clay brick infills. However, stiffness contribution decreases with increasing building height, reducing the relative benefit of infills in taller frames. Infill walls significantly reduced displacement and storey drift across all configurations, while Base shear was increased. Displacement was reduced by 80% for the concrete infill in the 2-storey structure and by 73 % for the clay infill, and Base shear was increased by 690% and 664% respectively. However, the stiffness contribution decreased as building height increased. This is observed by concrete infill reducing displacement by 79.7% in a 2-storey structure, but reducing it by 50% in a 10-storey structure. This research, therefore, provides region-specific evidence for the inclusion of masonry infill effects in seismic design.

Keywords: Masonry infill walls, Reinforced concrete frame, Pushover analysis, Equivalent strut method

TABLE OF CONTENTS

LIST OF FIGURES

LIST OF TABLES

LIST OF ABBREVIATIONS

ASCE	American Society of Civil Engineers
DE	Design Earthquake
CDP	Concrete Damage Plasticity
CSI	Computers and Structures, Inc
ETABS	Extended Three-Dimensional Analysis of Building System
FE	Finite Element
FEA	Finite Element Analysis
FEMA	Federal Emergency Management Agency
MRF	Moment Resisting Frame
OOP	Out of Plane
PGA	Peak Ground Acceleration
PSHA	Probability Seismic Hazard Assessment
RC	Reinforced Concrete
SDG	Sustainable Development Goal
UHS	Uniform Hazard Spectrum
UNBC	Uganda National Building Code
USGS	United States Geological Survey

SYMBOLS

S_S	Spectral acceleration at short periods
S_1	Spectral acceleration at 1s
F_a	Short-period site coefficient (ASCE 7-22)
F_v	Long-period site coefficient (ASCE 7-22)
S_{MS}	Site-adjusted spectral acceleration at short-period
S_{M1}	Site-adjusted spectral acceleration at 1 second
S_{DS}	Design spectral acceleration at short periods
S_{D1}	Design spectral acceleration at 1 second
T_S	Transition period
T_L	Long-period transition
E_m	Elastic Modulus of Masonry infill
f_m	Characteristic compressive strength of masonry infill
f_b	Characteristic compressive strength of Block or Brick
f_m	Characteristic compressive strength of mortar
λ	Relative stiffness parameter of masonry panel to the frame
t	Thickness of the wall
θ	Slope of diagonal of infill to horizonatal
E_c	Elastic Modulus of Concrete
I_c	Moment of Inertia
h_m	Height of infill wall
d_m	Beam depth
d	Length of diagonal strut
w	Width of diagonal strut

ACKNOWLEDGMENTS

This work stands as a testament to the incredible individuals whose steadfast support and guidance have shaped every step of this journey.

I would like to express my heartfelt gratitude to my supervisors, Dr. Moses Matovu and Dr. Allan Okodi, for their unwavering guidance, encouragement, and insightful feedback throughout the course of this research. Their expertise and support have been instrumental in shaping the quality and direction of this thesis.

I am also deeply thankful to my father, Mr. Baguma Gastone, whose generous financial support and belief in my academic journey made it possible for me to undertake and complete this project. Lastly, I extend my sincere appreciation to myself for the commitment, resilience, and perseverance that enabled me to see this work through to the end.

CHAPTER 1: INTRODUCTION

1.1 Background

Reinforced concrete frames are a network of columns and beams that form the structural skeleton of a building. They are widely used in building construction due to their strength, durability, versatility, and cost-effectiveness (Bilgin & Plaku, 2024). Infill masonry walls, typically made of different materials like clay bricks or concrete blocks, are commonly employed in Reinforced Concrete structures for purposes like partitioning and thermal insulation (Nour et al., 2023). During Seismic design of these structures, many practicing engineers assume that the infill walls are non-structural walls, that is, the wall's lateral contribution to the structure is ignored (Nour et al., 2022). However, masonry infill walls will interact with the surrounding frame in the event of an earthquake. Therefore, excluding this effect can lead to an inaccurate prediction of the structure's seismic response. Consequently, many have argued that the only feasible way to account for the positive and negative effects of infill walls is to directly include them in the analytical models used for seismic design and assessment purposes (Pallarés et al., 2021).

Earthquakes are among the most devastating natural disasters, resulting in significant loss of life, extensive infrastructure damage, and substantial economic disruption worldwide. According to the United States Geological Survey (USGS), approximately 500,000 detectable earthquakes occur annually, with about 100 causing significant damage (USGS, 2023). When improperly integrated or neglected in design, infills can induce undesirable failure modes. For instance, the 2009 L'Aquila earthquake showed that infill walls contributed to 30% of building collapses due to out-of-plane failures, while in the 2015 Nepal earthquake, infill-wall interaction caused 40% of RC frame damage (FEMA P-58, 2018). Between 2000 and 2023, earthquakes caused over $500 billion in economic losses globally, while RC structures account for 65% of building collapses in urban seismic zones (Delforge et al., 2025).

Africa is often perceived as having low seismicity, but several active rift zones, like the East African Rift and intraplate faults, pose significant hazards. The continent experiences about 900 earthquakes annually majority being moderate earthquakes, with magnitudes ranging from Mw 3.0 to Mw 7.0 (Bantidi, 2023). In North Africa, the Mediterranean seismic belt affects Morocco, Algeria, and Egypt, and this has caused earthquakes like the 2003 Boumerdès earthquake, Mw 6.8, which caused 2,300+ deaths and $5 billion in damages (Poggi et al., 2020; Khiatine et al., 2025). Earthquakes in Africa have a higher mortality rate per event compared

to global averages due to poor construction quality (Bantidi, 2023). Between 1990–2023, seismic events caused $12 billion in damages across Africa, with 70% of losses attributed to RC structure failures (Ackomah et al., 2024).

Uganda, situated in the East African Rift Valley, is prone to seismic activity due to its location within the Great Rift Valley system (Oleng et al., 2024). While major earthquakes are relatively infrequent in Uganda compared to other seismically active regions, the potential impact of even moderate seismic events on the built environment underscores the importance of seismic resilience in the country's construction practices (Cheriberi & Yee, 2022). Historically, Uganda has experienced several seismic events, one of the highest being a 6.6 magnitude earthquake in the Rwenzori region in 1966 that caused 160 deaths, 1300 injuries, and the destruction of over 7000 houses. One of the more current events that had a high economic loss was the 2016 Bukoba earthquake, which was of a 5.9 magnitude, and was felt in Rakai district, leading to the loss of 4 lives and affecting over 590 people (Oleng et al., 2024).

1.2 Problem Statement

In Uganda, the seismic vulnerability of structures poses a significant threat to public safety and infrastructure resilience. Despite this vulnerability, current seismic design practices in the country often treat masonry infill walls as non-structural elements, neglecting their complex interaction with reinforced concrete frames. Uganda’s seismic code also lacks detailed provisions for modelling and accounting for infill-wall interactions. The problem stems from a lack of comprehensive understanding of how infill masonry walls influence the seismic response of reinforced concrete frames in the context of Uganda's unique seismic conditions and construction practices.

Consequently, there is a pressing need to investigate how locally sourced, infill materials influence the seismic performance of RC frame structures in Uganda’s unique construction and seismic environment. Addressing this problem requires rigorous research efforts to investigate the interaction between infill masonry walls and reinforced concrete frames under seismic loading conditions specific to Uganda. By gaining insights into the behaviour of such structures, it is possible to mitigate the seismic risk and enhance the resilience of buildings in Uganda to seismic hazards.

1.3 Objectives

1.3.1 Main Objective

To investigate the influence of Masonry infill walls on the Seismic Response of Reinforced Concrete frame structures in Uganda.

1.3.2 Specific Objectives

i. To determine a site-specific design response spectrum for Uganda's highest seismic zone.
ii. To develop representative numerical models of Reinforced Concrete frames with and without masonry infills.
iii. To determine the seismic response of the numerical models under seismic loading by carrying out a pushover analysis.

1.4 Research Questions

1. What is the site-specific design response spectrum for Uganda's highest seismic zone?
2. What are the representative numerical models of Reinforced Concrete frames with and without masonry infills?
3. What is the seismic response of the numerical models under seismic loading when carrying out a pushover analysis?

1.5 Significance

The seismic performance of reinforced concrete frame structures is profoundly influenced by the presence of masonry infill walls, yet their contribution is often overlooked in conventional structural design, particularly in regions of low to moderate seismicity such as Uganda.

This study provides critical insights into the role of masonry infill in enhancing the lateral stiffness, strength, and overall seismic resilience of RC buildings, thereby addressing a significant gap in the understanding of infill-frame interaction in Uganda, where empirical data is scarce. Additionally, this study advocates for the explicit inclusion of masonry infill effects in structural analysis to prevent inaccurate seismic responses during design.

Ultimately, this study not only advances the regional understanding of infill-frame systems but also provides actionable recommendations for safer, more resilient building practices in seismically vulnerable developing nations, where informal construction often neglects such critical considerations.

By aligning analytical models with localized material properties and seismic demands, this research sets a precedent for evidence-based seismic design in regions where empirical data is limited but the consequences of seismic vulnerability are disproportionately high.

1.6 Justification

The seismic vulnerability of reinforced concrete (RC) frame structures with masonry infill walls remains a critical yet understudied issue in Uganda and similar regions, where rapid urbanization and informal construction practices often neglect proper seismic design considerations.

This study is justified by its alignment with Sustainable Development Goal (SDG) 11, which aims to "make cities and human settlements inclusive, safe, resilient, and sustainable." Given that Uganda lies in a region of moderate seismicity and lacks robust building codes that account for masonry infill effects, many structures are at risk of disproportionate damage during earthquakes, thereby threatening lives and economic stability. Therefore, this research also directly supports SDG Target 11.5, which seeks to "significantly reduce the number of deaths and economic losses caused by disasters."

This research contributes to SDG Target 11.b, which calls for integrated policies to reduce disaster risks. By bridging the gap between experimental research and practical design applications, this study not only advances structural engineering knowledge but also fosters disaster-resilient infrastructure, ultimately safeguarding communities and supporting sustainable urbanization in seismically vulnerable regions.

1.7 Conceptual framework

The conceptual framework of this study, as shown in Figure 1.1, establishes a structured approach to investigate how masonry infill walls influence the seismic performance of reinforced concrete frame structures in Uganda. The independent variables include building height and masonry type, specifically hollow concrete blocks and solid clay bricks, which were varied to assess their impact on structural behaviour. Intervening variables, such as storey height, geometrical and material properties of the RC frame, gravity loads, and local soil conditions, are accounted for to ensure realistic modelling. The process involves three key steps: developing a design response spectrum tailored to Uganda’s seismic conditions, creating numerical models of the RC frames with and without infill, and performing pushover analysis to evaluate nonlinear seismic response. The dependent variables: storey displacement, storey drift, and base shear, serve as critical performance indicators, quantifying the effect of infill walls on seismic resilience. This framework ensures a comprehensive assessment of infill-wall

contributions across different building heights and masonry types, providing actionable insights for safer seismic design practices in Uganda.

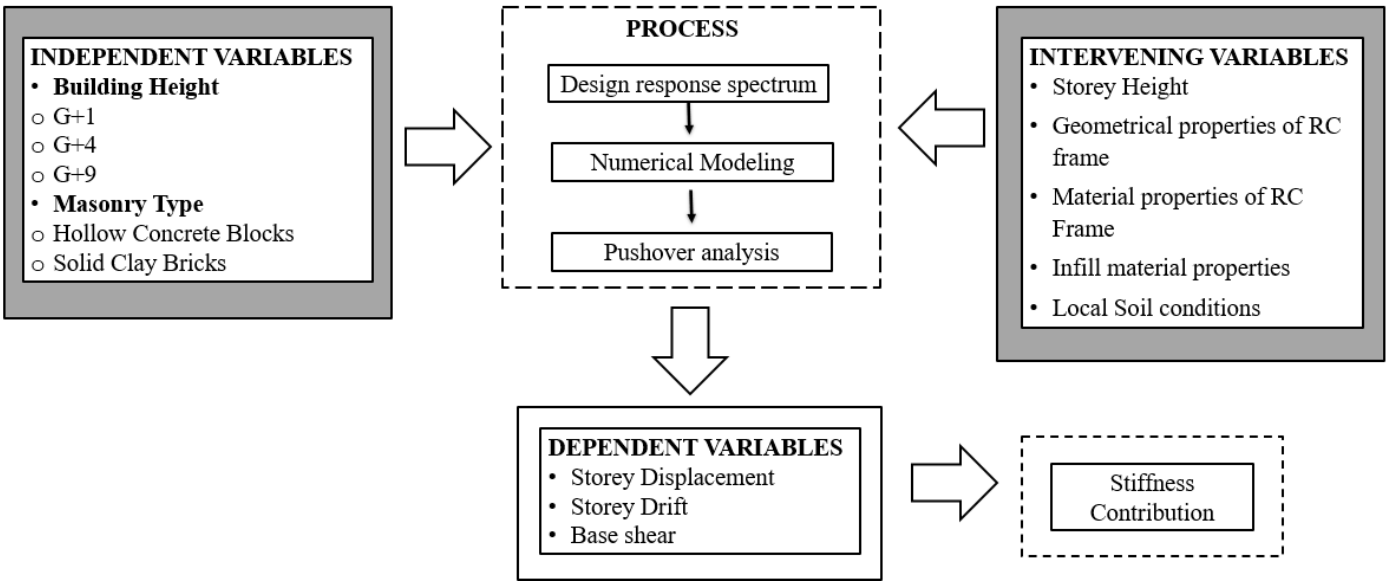

Figure 1.1 Conceptual framework

1.8 Scope of the Study

This section outlines the boundaries and main areas of the study, clarifying what the research includes. It defines the content scope under consideration and the geographical area to which the findings are most applicable. This helps contextualize the study within Uganda's construction practices and seismic risk profile.

1.8.1 Content scope

This study covers the investigation of the influence of masonry infill walls on the seismic performance of RC frame structures within the context of Uganda. It considers typical Ugandan construction practices and materials, particularly using commonly available masonry types such as clay bricks and concrete blocks.

The research uses numerical modelling techniques, particularly finite element analysis in ABAQUS and equivalent diagonal strut modelling in ETABS. These models simulate the behaviour of RC frames with and without masonry infill under seismic loading. The study specifically examines low-rise (G+1), mid-rise (G+4), and high-rise (G+9) building configurations, considering in-plane, uniformly distributed masonry infill.

1.8.2 Geographical scope

The geographical focus of this research is Uganda, with particular emphasis on Zone 1, the highest seismic risk area in the country as defined by Uganda's seismic zoning map in US 319:2003. This is part of the Rwenzori sub-region, located along the Western Rift Valley, an

area prone to significant seismic activity due to its tectonic setting in the East African Rift System.

By focusing on Zone 1, the study sought to address the most severe seismic conditions in Uganda, based on the premise that a structure designed to endure the forces in this highest-risk area would be sufficiently robust to perform well in all other seismic zones within the country. This ensures that the findings and recommendations of the study are grounded in Uganda's actual seismic context and can be directly applied to enhance earthquake-resistant construction practices in the region.

CHAPTER 2: LITERATURE REVIEW

2.1 Overview

The influence of infill masonry walls on the seismic performance of reinforced concrete (RC) frames has been a subject of extensive research due to its significant impact on the structural behaviour during earthquakes, and has been studied for more than 50 years (Morandi et al., 2017). This literature review looks into key findings from previous studies, focusing on the behaviour of infill masonry walls in RC frames, the methodologies employed in their analysis, and the implications for seismic design.

2.2 Masonry Walls

Masonry walls are structural or non-structural systems constructed using individual units bonded together with mortar, forming a durable and robust building element. These walls have been utilised for centuries due to their strength, fire resistance, and aesthetic versatility (Lakshani et al., 2020). The primary materials used in masonry construction include bricks, concrete blocks, stone, and clay tiles, each offering distinct structural and thermal properties (Thaickavil & Thomas, 2018). Bricks, for instance, are highly durable and provide excellent thermal mass, while concrete blocks are favoured for their cost-effectiveness and ease of installation.

Stone masonry, though labour-intensive, delivers unparalleled longevity and aesthetic appeal, often seen in historical and high-end architectural projects (Vijayan et al., 2021; Akinradewo & Adedokun, 2020; Arêde et al., 2019). The mortar, typically composed of cement, lime, sand, and water, acts as the binding agent, ensuring cohesion between units while accommodating slight movements and stresses (Lakshani et al., 2020).

Despite their advantages, masonry walls require careful detailing to address potential issues such as moisture penetration, thermal bridging, and cracking due to settlement or thermal expansion. Proper waterproofing, insulation, and expansion joints are essential to ensure long-term performance (Vijayan et al., 2021). Masonry walls remain a fundamental component of construction, combining tradition with innovation to meet contemporary architectural and engineering demands. Their adaptability, durability, and aesthetic flexibility ensure their continued relevance in both residential and commercial building projects (Thaickavil & Thomas, 2018).

2.3 Non-Structural walls

Masonry infill walls are non-structural walls used to enclose reinforced concrete frame structures, providing thermal, acoustic, and aesthetic benefits without contributing to the gravity load-bearing capacity (Milijaš et al., 2024). In typical RC frame construction, the structural frame is built first, followed by the installation of masonry infill panels, which are primarily made of brick or concrete blocks. Since the RC frame independently supports vertical loads, the removal of infill walls does not compromise the structural integrity of the building (Borah et al., 2023).

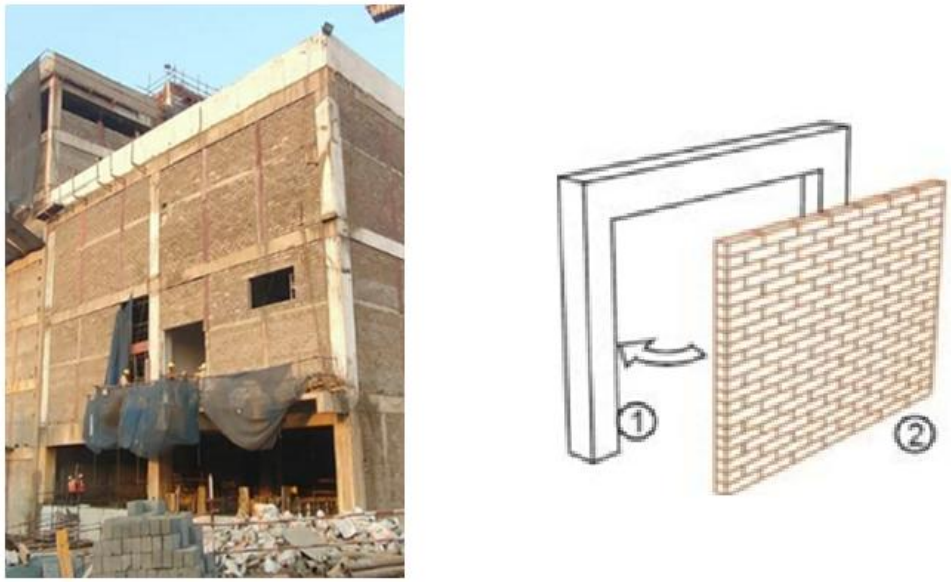

Figure 2.1 Masonry infill structure

One notable characteristic of masonry infill walls is the presence of gaps between the top of the wall and the underside of the RC beams. These gaps occur due to construction tolerances or intentional design to prevent load transfer from the beams to the infill. This separation allows the beams to deflect under vertical loads without imposing additional stresses on the masonry (Sen & Chowdhury, 2024). However, under lateral loads such as wind or seismic forces, the interaction between the RC frame and the infill becomes more complex. The frame tends to deform in a flexural manner, while the infill panels primarily resist shear stress, leading to a gap formation at the tension corners and the activation of the equivalent diagonal compression strut across the infill (Borah et al., 2023). During earthquakes, infill walls often behave as diagonal compression struts, altering the structural response by increasing stiffness and strength but also potentially inducing brittle failure modes if not properly accounted for in

design. This strut action can lead to localised damage, such as cracking in the masonry or even collapse of the infill (Nour et al., 2023).

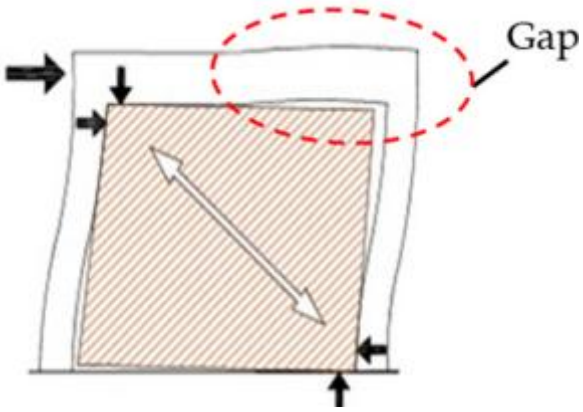

Figure 2.2 Behaviour of a masonry infill wall subjected to lateral loading

2.4 Behaviour of Infill Masonry Walls in RC Frames

2.4.1 Strength and Stiffness Contribution

Masonry infill walls contribute to the overall stiffness and strength of RC frames, which can enhance their seismic performance if properly designed and detailed. However, the contribution of infill walls is highly dependent on their connection to the surrounding frame and their material properties (Khan et al., 2019). Generally, the contribution of infills to the overall capacity of structures is strongly dependent on the regularity of their distribution in plan and over height. A regular distribution of infills has a beneficial effect, especially for non-seismic designed buildings, increasing their global bearing capacity and stiffness under lateral actions (Milijaš et al., 2024).

Infill walls enhance the lateral load-bearing capacity of RC frames. They act as compression members, effectively transferring lateral loads through diagonal struts formed within the infill material (Nour et al., 2023). The research by Zine et al., (2021) demonstrates that infill walls can significantly increase the lateral load resistance, thereby reducing the demand on the RC frame elements. Infill walls also contribute to the energy dissipation capacity of the structure during seismic events. Their presence can reduce the amplitude of lateral displacements, as they absorb and dissipate seismic energy through inelastic deformation and cracking (Moreira et al., 2023). Studies such as those by Pallarés et al., (2021) have shown that properly designed infill walls can enhance the overall ductility and energy dissipation of RC frames, leading to improved seismic performance. The distribution of lateral forces is altered by the presence of infill walls. The walls can create a more uniform distribution of seismic forces across the

structure, reducing the likelihood of localised failures in columns and beams (Umar et al., 2020).

Infill masonry walls significantly increase the initial stiffness of RC frames, which is the primary resistance against small seismic forces. The increased stiffness reduces the lateral displacements and inter-story drifts at lower seismic intensity levels (Khan et al., 2019). This initial stiffness enhancement is particularly beneficial in minimizing damage to non-structural elements during low to moderate seismic events. The addition of infill walls modifies the dynamic characteristics of the structure, including the natural frequencies and mode shapes. This modification can result in a higher natural frequency, thereby potentially reducing the seismic demand on the structure.

While infill walls contribute to the initial stiffness, their stiffness degrades with increasing seismic loads due to cracking and potential crushing of the masonry. Studies by Zine et al., (2021) and Pallarés et al., (2021) indicate that this stiffness degradation must be considered in the design process to avoid overestimating the seismic performance of infill walls. The cyclic behaviour and the progressive loss of stiffness during seismic events need to be accurately modelled to predict the structure's behaviour under severe seismic loading.

2.4.2 Failure Mechanisms

The behaviour of infill masonry walls within reinforced concrete (RC) frames under seismic loading involves complex interactions that can lead to various failure mechanisms. Understanding these failure mechanisms is crucial for designing structures that can withstand seismic forces without catastrophic collapse.

2.4.2.1 In-Plane failure

One of the most common failure mechanisms in infill masonry walls is diagonal cracking. As the lateral loads increase, the infill wall tends to act as a diagonal compression strut between the corners of the RC frame. This strut action induces tensile stresses along the diagonal, leading to the formation of diagonal cracks as shown in Figure 2.3. Islam & Sen, (2023) have documented that diagonal cracking often initiates at lower seismic forces and can significantly affect the stiffness and load-bearing capacity of the structure. This failure mechanism is particularly prevalent in infills with weak mortar joints or low-quality masonry units, where the bond strength between bricks or blocks is insufficient to resist shear deformation. The formation of diagonal cracks reduces the effective stiffness of the infill panel, leading to a gradual degradation in lateral load resistance (Khokhar & Brzev, 2021).

The corners of infill masonry walls are particularly susceptible to crushing under seismic loads, as seen in Figure 2.4. The concentrated stresses at the corners, where the diagonal strut action is most pronounced, can exceed the compressive strength of the masonry material, leading to corner crushing (Dias-Oliveira et al., 2022). This phenomenon is exacerbated in cases where the frame undergoes significant deformation, forcing the infill into a highly compressed state. Corner crushing often leads to a sudden drop in strength and can trigger secondary failures, such as the buckling of the diagonal strut or spalling of the surrounding concrete (Mucedero et al., 2022).

Infill walls can also experience sliding shear failure along horizontal joints or at the interface with the RC frame. This type of failure is characterised by the relative sliding of the wall segments or the entire wall along a plane of weakness. Islam & Sen, (2023) noted that sliding shear failure is often precipitated by inadequate shear transfer mechanisms and poor interface bonding.

Figure 2.3 Diagonal Cracking

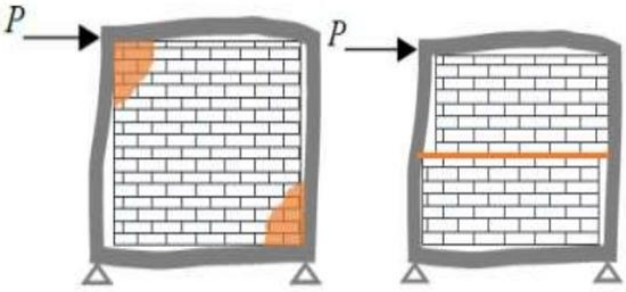

Figure 2.4 Corner Cracking and Sliding shear

2.4.2.2 Out-of-plane Failure

Masonry infill walls, while primarily designed to resist in-plane lateral loads, are also vulnerable to out-of-plane failure under seismic excitation. Unlike in-plane behaviour, where

the infill acts as a diagonal compression strut, OOP failure occurs when inertial forces perpendicular to the wall plane induce bending and instability (Guettala et al., 2023). The separation of the infill wall from the surrounding RC frame is a critical failure mechanism which often occurs at the interface due to inadequate bonding or differential movement between the frame and the wall. This separation can lead to a significant reduction in the composite action between the wall and the frame, thereby decreasing the overall lateral stiffness and strength of the structure (Morandi et al., 2021).

Infill walls, particularly slender ones, can experience out-of-plane buckling under seismic loading as seen in Figure 2.5. This failure mode is influenced by the slenderness ratio of the wall and the degree of lateral support provided by the frame. Research by Xie et al., (2021) indicates that out-of-plane buckling can lead to a sudden and brittle collapse of the infill wall, posing a serious risk to the overall stability of the structure.

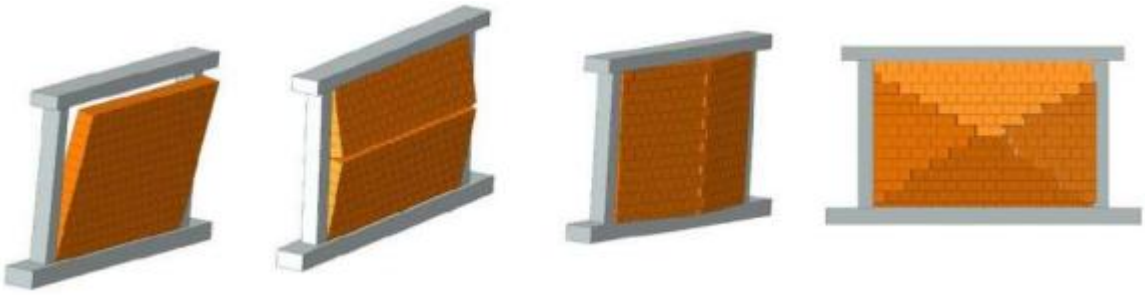

Figure 2.5 Out-of-plane failure modes of masonry infill

2.4.2.3 Other Failure Mechanisms

Soft storey collapse

Irregular distributions of panels may be dangerous. They can cause a potential collapse when seismic events occur. When irregular distribution of infills occurs over the height of buildings, it generally produces strong differences of storey strength and stiffness, being the potential cause of soft storey collapse mechanisms (Milijaš et al., 2024). In this case, the damage is concentrated only in the storeys where infills are missing, with fatal consequences. Moreover, it should also be noted that even if the distribution of infills is regular in plan and over the height, the increase of stiffness causes higher restoring forces that should be carried by the infill panels (Khan et al., 2019). The effects caused by the local interaction require the frame elements to have a bearing capacity that can exceed design values to support the increased efforts transferred by the infill. Especially in the case of low shear reinforced elements without seismic detailing, this may cause local brittle shear collapses of the columns and even of the nodes, strongly compromising the overall capacity (Mucedero et al., 2022).

Column collapse in shear

Other collapse mechanisms due to the infill–frame interaction occur when infills present openings adjacent to the column in such a way that the panel is shorter than the column itself (Dias-Oliveira et al., 2022). This fact modifies the design length of the column, causing an unexpected increase of local shear demand. In these cases, the columns undergo an anticipated collapse that depends on the aspect ratio and on the free length of the column. If the columns are squat, shear failure occurs, otherwise, the collapse is due to a double plastic hinge mechanism (Islam & Sen, 2023).

(a) (b)

Figure 2.6 a) Soft storey Collapse b) Column Failure

2.5 Methodologies for Analysing Infill Masonry Walls

The analysis of reinforced concrete frames with infill masonry walls under seismic loading involves complex interactions that are challenging to model accurately. Various analytical models have been developed to simplify these interactions and provide practical tools for engineers to predict the seismic performance of these composite structures. In the last decades, several researchers provided experimental and analytical studies proposing modelling strategies to predict and introduce in practical technique the above-discussed interaction effects. From a general point of view, the infill–frame interaction has been substantially faced by two main approaches: macromodelling and micromodelling (Guettala et al., 2023). This is represented schematically in Figure 2.7 below.

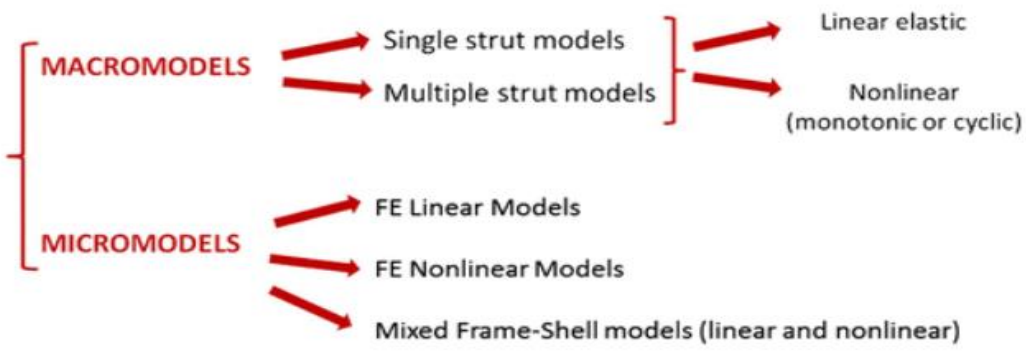

Figure 2.7 Analysis models

2.5.1 Macromodel

The macromodel approach involves replacing masonry infills with one or more equivalent pin-jointed struts for each infill as shown in Figure 2.8. This technique is the most frequently used in practice to perform linear/nonlinear static or dynamic analyses because of its simplicity and lower computational effort required (Guettala et al., 2023).

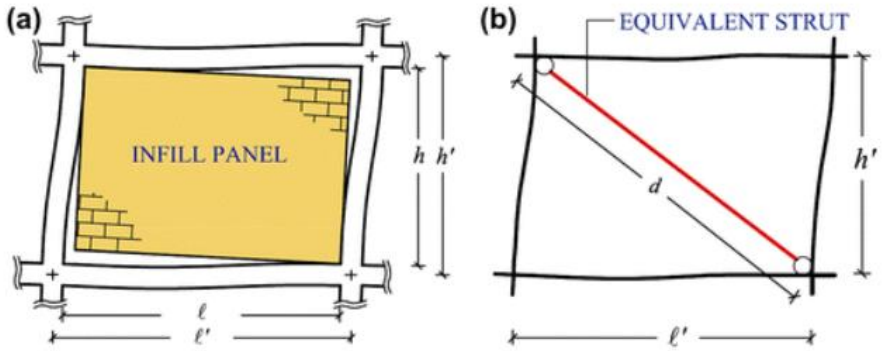

Figure 2.8 Macro model approach

Besides the attribution of geometrical dimensions of the cross-section, the identification of the equivalent diagonal strut requires the assignment of specified mechanical characteristics for the strut, depending on the properties of the actual system (Moreira et al., 2023). Especially for masonry infills of existing buildings, the identification of the necessary information is affected by a large uncertainty since this depends not only on masonry properties but also on manufacturing and local arrangement details. In a few words, the macromodel should summarise all these aspects with a single strut able to account for strength, stiffness, and damage (Bagnoli et al., 2022).

The first studies on this topic are due to Holmes, (1961), who worked with brick masonry infilled steel frames. He proposed the empirical rule to replace the panel with an equivalent diagonal strut, having a cross-sectional width w equal to 1/3 of the diagonal length d.

Afterwards, several other researchers proposed more detailed methods, mainly basing the identification of the equivalent width on the ratio between the elastic characteristics of the infill and the surrounding frame, like Mainstone, (1971).

The single-strut macromodels represent the easiest way to introduce the presence of infill panels in models in practical engineering. They are suitable for the analysis of complex structures and are easy to identify. They are, moreover, able to provide a good approximation despite their simplicity. Their limit mainly lies in the concentric configuration of the equivalent strut, which makes it not possible to account for the shear transmission in critical sections (Bagnoli et al., 2022).

2.5.2 Micromodeling

Detailed FEA has been used to capture the nonlinear behaviour and complex interactions within the RC frame-infill wall system. Studies by Dhir et al., (2021) and Roudane, (2019) utilized FEA to model the cyclic behaviour of infill walls, considering factors such as material nonlinearity and bond-slip effects. These models provide insights into the detailed failure mechanisms and stress distributions within the infill walls and frames.

FE micromodels represent the most accurate approach to capture the frame–infill interaction, being also the most similar to the real physics of the problem. Besides the stiffening effects, micromodels can, through interface elements, represent complex issues such as the local frame–infill interaction, the sliding of the units along mortar joints, the cracking propagation on infills and reinforced concrete elements (Bagnoli et al., 2022).

Although this advantage, they still present a double difficulty. The first one regards a proper calibration that may be really difficult to provide, requiring, especially for nonlinear cases, the knowledge of several parameters and sufficient experience to handle this kind of modelling. The second, and more relevant, is related to the high computational effort needed (Guettala et al., 2023).

2.6 Seismic response

The seismic response of a structure refers to its behaviour when subjected to ground motions caused by earthquakes. This response is influenced by factors such as the building's mass, stiffness, damping characteristics, foundation type, and the frequency content of the seismic waves (Chen & Chen, 2023). When an earthquake occurs, the ground shakes, imparting inertial forces to the structure, which then vibrates in dynamic modes. Engineers analyse this response to ensure that buildings remain stable, avoid excessive deformations, and prevent collapse (Kia et al., 2021). Key response parameters include lateral displacements, drift, base shear, storey

shear, and floor accelerations. Excessive displacements can lead to storey drift failures, while high accelerations may damage non-structural components like facades and partitions (Petreski & Gjorgjiev, 2021).

Understanding seismic response is crucial for performance-based design, where structures are engineered to meet specific objectives, such as remaining operational after minor earthquakes or preventing collapse in extreme events (Chen & Chen, 2023). Advances in computational modelling, shake table testing, and real-time monitoring continue to refine seismic analysis, improving the resilience of buildings and infrastructure in earthquake-prone regions. (Stojadinović et al., 2022) By integrating robust design principles with innovative technologies, engineers can enhance a structure's ability to withstand seismic forces, protecting lives and property.

2.6.1 Pushover analysis

Pushover analysis is a nonlinear static analysis method used to evaluate the seismic performance of structures. It involves applying a progressively increasing lateral load pattern to a structural model until a specified target displacement is reached or the structure collapses. The primary objective is to understand the inelastic behaviour, identify failure mechanisms, and estimate the overall capacity of the structure (Ashwini et al., 2024).

A predefined lateral load pattern, typically representing seismic forces, is applied incrementally. Common patterns include uniform, triangular, or modal-based distributions. The analysis generates a capacity curve or pushover curve, which plots the base shear force against the roof displacement (Mandal, 2023). This curve illustrates the structure's ability to withstand lateral forces and provides insights into its stiffness, strength, and ductility. The intersection of the capacity curve with the demand curve (representing seismic demand) identifies the performance point, which indicates the expected performance level of the structure during an earthquake (Toufik & Salah, 2024).

Pushover analysis is widely used to assess the seismic performance of RC frames with infill masonry walls due to its ability to capture the nonlinear behaviour and failure mechanisms of these composite systems (Mandal, 2023). By comparing the capacity curves of frames with and without infill walls, engineers can assess the extent to which infill walls enhance the seismic performance. (Nour et al., 2023).

2.6.2 Storey Drift

Storey drift is a critical parameter in structural engineering that refers to the lateral displacement of one level of a building relative to the level below it when subjected to lateral

loads such as wind or seismic forces. It is typically expressed as a ratio of the inter-storey displacement to the storey height and is a key measure of a building's performance under dynamic loading (Hori et al., 2022). Excessive storey drift can lead to non-structural damage, such as cracked partitions and broken cladding, and in severe cases, can compromise the structural integrity of the building by causing instability or failure of load-bearing elements (Al-hagri et al., 2023).

Building codes, such as ASCE 7 and Eurocode 8, prescribe allowable drift limits to ensure safety and serviceability, with stricter limits for seismic zones to prevent collapse during earthquakes. Engineers control storey drift through proper structural design, including the use of shear walls, braced frames, moment-resisting frames, or damping systems to enhance stiffness and energy dissipation (Etemadi & Balkaya, 2024). Advanced analysis techniques, such as nonlinear time-history analysis, are often employed to accurately predict drift behaviour under extreme loading conditions (Petreski & Gjorgjiev, 2021). Effective drift management ensures occupant comfort, minimises repair costs, and enhances the resilience of structures against natural hazards.

2.6.3 Base shear

Base shear capacity is the maximum total lateral force at the base of a structure that it can resist. Base shear is the total lateral force that a building experiences at its base due to dynamic loads such as earthquakes or wind. It represents the maximum expected inertial force generated by the building's mass when subjected to ground motion and is therefore influenced by mass, stiffness, and dynamic characteristics (Nour et al., 2022); (Ramachandra et al., 2020). Building codes, such as ASCE 7, Eurocode 8, and IS 1893, provide empirical formulas to estimate base shear using parameters like seismic zone coefficients and the structure's fundamental period. The added mass of a building generates higher inertial forces under seismic excitation, leading to a marked increase in base shear demands (Pudjisuryadi et al., 2021).

Beyond the influence of mass, a structure's dynamic characteristics can be influenced by increasing its lateral stiffness. This stiffening effect typically results in a higher natural frequency and a shorter fundamental period of vibration, which often positions the structure in a region of higher spectral acceleration within a design response spectrum, resulting in increased inertia forces and, consequently, higher base shear demand (Xie et al., 2020).

2.7 Literature review summary

The existing literature demonstrates that masonry infill walls influence the seismic response of reinforced concrete frames by enhancing strength and energy dissipation capacity, while also

introducing complex failure mechanisms such as diagonal cracking, sliding shear, and soft-storey effects. Analytical approaches, including macromodelling and micromodelling, have been developed to simulate this behaviour with varying levels of accuracy and computational demand. However, despite these findings, there remains a gap in the application of this knowledge to places where seismic design codes lack explicit provisions for infill-frame interaction and where local construction materials, and seismic characteristics differ from those in previously studied regions.

This study addresses these gaps by developing a site-specific design response spectrum for Uganda's highest seismic zone and by incorporating locally relevant masonry materials, such as clay bricks and concrete blocks, into the analysis. Furthermore, it combines detailed finite element modelling with the practical equivalent diagonal strut approach to evaluate the nonlinear seismic behaviour of RC frames across different building heights. By doing so, the research provides specific insights into displacement, storey drift, base shear, and stiffness contributions. Ultimately, this study contributes to improving seismic design approaches in Uganda by offering evidence-based recommendations for incorporating masonry infill effects into structural analysis and design.

CHAPTER 3: METHODOLOGY

3.1 Research Design

This research project investigates the influence of masonry infill walls on the seismic response of reinforced concrete frame structures in Uganda through numerical modelling and comparative analysis. Reinforced Concrete models with and without masonry infill were designed using the ABAQUS and ETABS software. Thereafter, a pushover analysis was carried out on these models, which were then analysed from their corresponding seismic response.

3.2 Uganda's active seismic zones

Uganda is divided into three seismic zones, as shown in Figure 3.1, with Zone 1 having the highest seismic activity. This is because Zone 1 is in western Uganda, which is situated in the East African rift Valley system, which experiences a lot of seismic activity due to tectonic forces associated with the East African Rift System (Cheriberi & Yee, 2022).

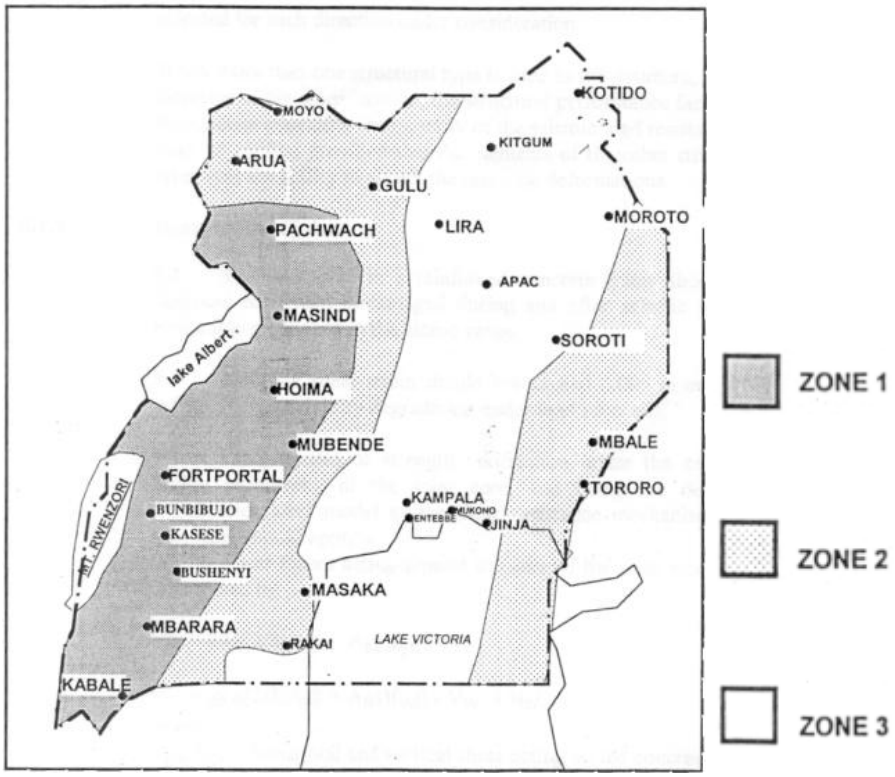

Figure 3.1 Map showing seismic zones of Uganda

The probabilistic seismic hazard assessment (PSHA) by Oleng et al., (2024) identifies Fort Portal as a high-seismicity region within the Western Rift System, with a peak ground acceleration (PGA) of 0.255 g for a 475-year return period with a 10% probability of exceedance in 50 years. Fort Portal, located in the Toro sub-region of Western Uganda in

Kabarole District, as shown in Figure 3.2, is situated near the Rwenzori Mountains and along the Albertine Rift, which is a section of the larger Western Rift Valley.

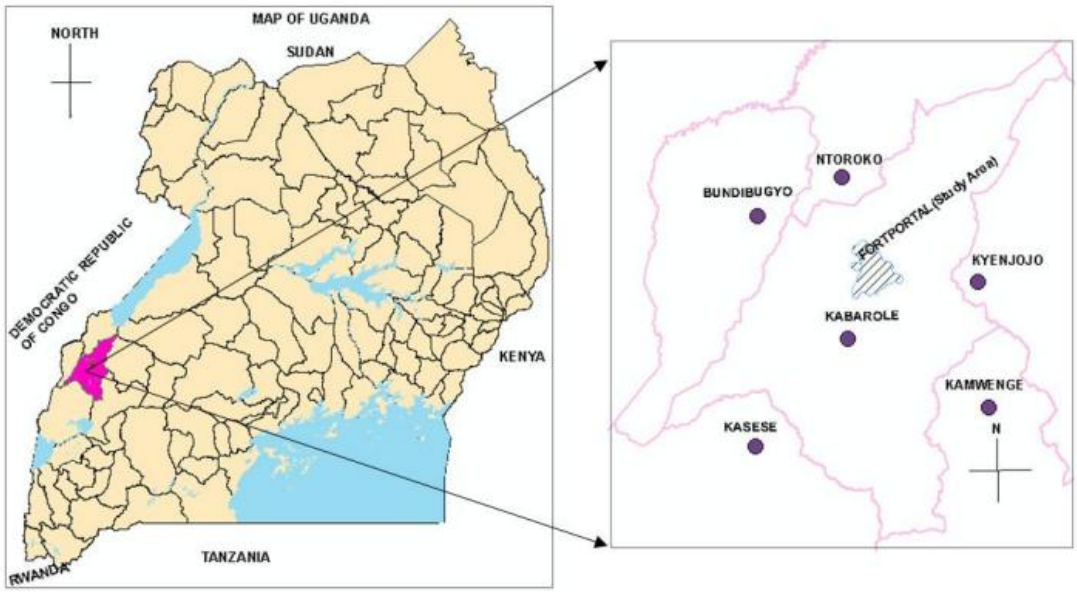

Figure 3.2 Location of Fort Portal in Uganda and its neighbouring districts

3.3 Determining Fort Portal's Design Response Spectrum

The design spectrum was developed in accordance with the American seismic code ASCE 7-22 (ASCE, 2022). The American code is widely recognised, well-documented and based on extensive seismic research, making it a reliable reference even for regions like Uganda that lack their detailed procedures. The Design Earthquake (DE) per ASCE 7-22, corresponding to a 475-year return period with 10% probability of exceedance in 50 years, had a bedrock Peak Ground Acceleration (PGA) of 0.255 g, as derived from bedrock hazard maps by Oleng et al., (2024). The spectral acceleration values were obtained from the mean Uniform Hazard Spectrum (UHS) for Fort Portal as shown in Figure 3.3, with an SS (short-period spectral acceleration parameter at 0.2 seconds) of 0.54g and an S1 (1-second spectral acceleration parameter) of 0.107g.

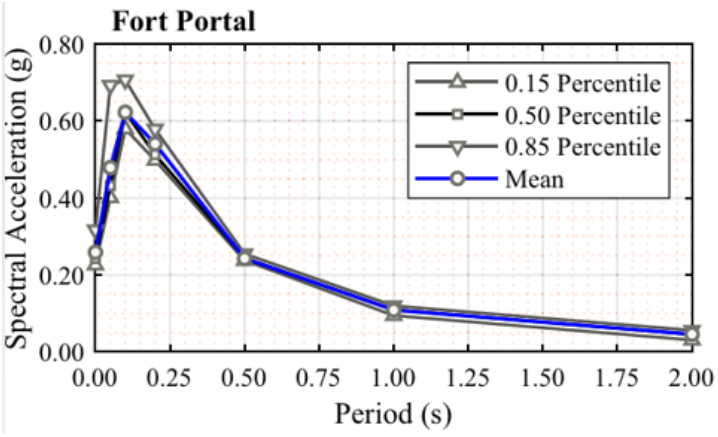

Figure 3.3 Mean and percentile Uniform Hazard Spectra of Fort Portal

Ss and S_1 were adjusted for site class effects to obtain the short-period maximum, S_{MS}, and 1-second period maximum, S_{M1}. The site was classified as Soil Class D according to ASCE 7-22, representing stiff soil conditions with a shear-wave velocity (vs,30) range of 180–360 m/s, to account for potential variability in Fort Portal's geotechnical data and the absence of site-specific vs,30 measurements. This approach aligns with the findings of Oleng et al., (2024), which indicated that Uganda's soil conditions, based on USGS-derived shear-wave Velocity data for the upper 30 m, predominantly correspond to stiff-soil profiles. The site coefficients, F_a and $F_{v,}$ were then read off from Tables 3-1 and 3-2 from the ASCE 7-22, and S_{MS} and S_{M1} were obtained.

Table 3-1 Site Coefficient, Fa

Site Class	Ss≤0.25	Ss=0.5	Ss=0.75	Ss=1	Ss≥1.25
A	0.8	0.8	0.8	0.8	0.8
B	1	1	1	1	1
C	1.2	1.2	1.1	1	1
D	1.6	1.4	1.2	1.1	1
E	2.5	1.7	1.2	0.9	0.9
F	Section 11.4.7				

Table 3-2 Site Coefficient, Fv

Site Coefficient, Fv					
Site Class	**S1≤0.1**	**S1=0.2**	**S1=0.3**	**S1=0.4**	**S1≥0.5**
A	0.8	0.8	0.8	0.8	0.8
B	1	1	1	1	1
C	1.7	1.6	1.5	1.4	1.3
D	2.4	2	1.8	1.6	1.5
E	3.5	3.2	2.8	2.4	2.4
F	Section 11.4.7				

$$S_{Ms} = F_a S_s \quad (3\text{-}1)$$

$$S_{M1} = F_v S_1 \quad (3\text{-}2)$$

Design earthquake spectral response acceleration at short periods, S_{DS}, and at 1-second period, S_{Dl}, were determined from the following equations,

$$S_{Ds} = \frac{2}{3} S_{Ms} \quad (3\text{-}3)$$

$$S_{D1} = \frac{2}{3} S_{M1} \quad (3\text{-}4)$$

The design response spectrum curve was developed as follows:

- For periods less than or equal to T_0, the design spectral response acceleration, Sa, was taken as given by;

$$S_a = S_{Ds}\left(0.4 + 0.6\frac{T}{T_0}\right) \quad (3\text{-}5)$$

Where; $T_0 = 0.2\frac{S_{D1}}{S_{Ds}}$ (3-6)

$$T = Fundamental\ period\ of\ vibration$$

- For periods greater than or equal to T_0 and less than or equal to the transition period (Ts), the design spectral response acceleration, Sa, was taken as equal to S_{DS}.

Where, $T_S = \frac{S_{D1}}{S_{Ds}}$ (3-7)

- For periods greater than Ts but less than the long-period transition (T_L), the design spectral response acceleration, Sa, was given by:

$$S_a = \frac{S_{D1}}{T} \quad (3\text{-}8)$$

- For periods greater than T_L, the design spectral response acceleration, Sa, was given by;

$$S_a = \frac{S_{D1}.T_L}{T^2} \quad (3\text{-}9)$$

Where T_L is 8 seconds, which is recommended for soils with soil class D, according to the ASCE 7-22.

Figure 3.5 shows a graphical representation of this procedure.

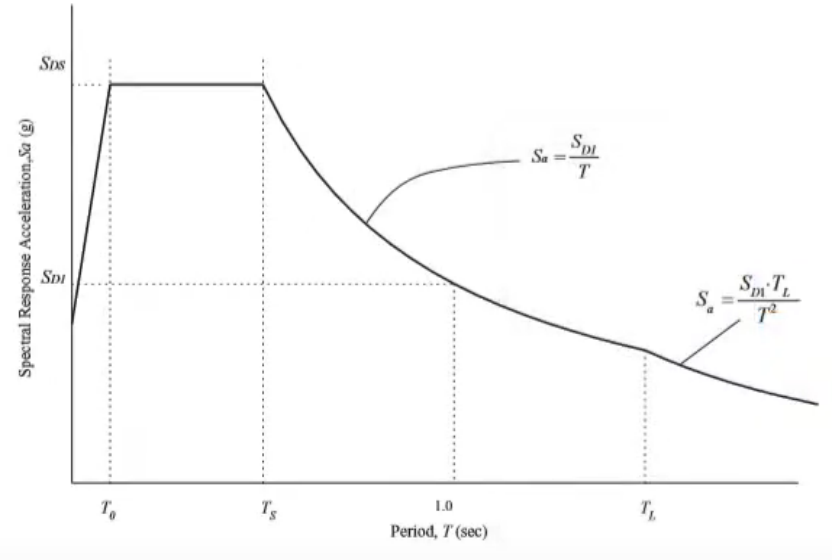

Figure 3.4 Design response spectrum piecewise function

Following this procedure, the Design spectrum was plotted in EXCEL.

3.4 Numerical Modelling Masonry infill

3.4.1 Overview of FEA modelling in Abaqus

The masonry infill was meticulously modelled using a detailed finite element (FE) approach in Abaqus/Explicit to accurately capture its local nonlinear behaviour and interaction with the surrounding reinforced concrete frame under seismic loading conditions. The model incorporated continuum elements with appropriate material definitions to simulate the infill's brittle response, while interface elements were employed to represent the contact and potential slip between the masonry and the RC frame. Material nonlinearity, geometric effects, and damage progression were accounted for through constitutive models such as the Concrete Damage Plasticity (CDP) for the RC frame and a Drucker-Prager model for the masonry, ensuring a realistic representation of infill behaviour under seismic demands.

3.4.2 Overview of Modelling in Etabs

The masonry infill was also modelled in ETABS by representing the masonry infill wall as a diagonal strut, as shown in Figure 3.6. The geometrical dimensions of the wall cross-section

were attributed to the equivalent diagonal strut, which also requires the assignment of specified mechanical characteristics for the strut, depending on the properties of the actual system.

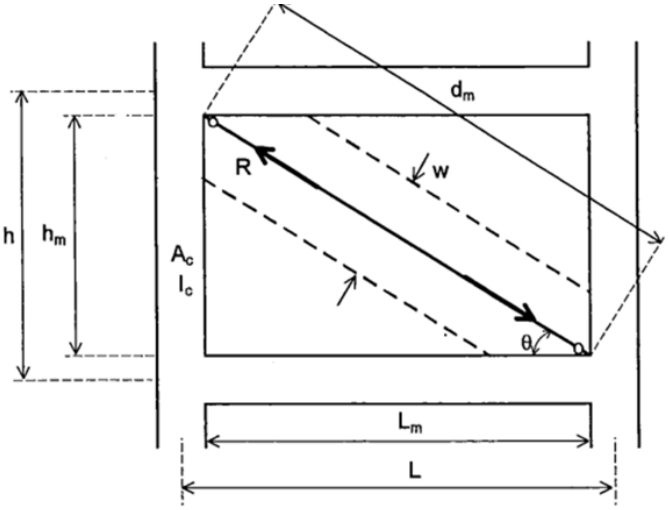

Figure 3.5 Equivalent Diagonal strut

The diagonal strut can be derived from a series of equations as shown below developed by Mainstone, (1971).

$$E_m = 550 f_m \tag{3-10}$$

$$f_m = 0.55 f_b^{0.7} f_{m0}^{0.3} \tag{3-11}$$

$$\lambda = \sqrt[4]{\frac{E_m t \sin 2\theta}{2 E_c I_c h_m}} \tag{3-12}$$

$$w = 0.175(\lambda h_m)^{-0.4} d \tag{3-13}$$

Where;

$E_m = Elastic\ Modulus\ of\ Masonry\ infill$

$f_m = Characteristic\ compressive\ strength\ of\ masonry\ infill$

$f_b = Characteristic\ compressive\ strength\ of\ Block\ or\ Brick$

$f_m = Characteristic\ compressive\ strength\ of\ mortar$

$\lambda = Relative\ stiffness\ parameter\ of\ masonry\ panel\ to\ the\ frame$

$t = thickness\ of\ the\ wall$

$\theta = Slope\ of\ diagonal\ of\ infill\ to\ horizonatal$

$E_c = Elastic\ Modulus\ of\ Concrete$

$I_c = Moment\ of\ Inertia$

$h_m = Height\ of\ infill\ wall$

$d_m = Beam\ depth$

$d = Length\ of\ diagonal\ strut$

$w = Width\ of\ diagonal\ strut$

3.5 Developing FE Model of RC Frame with and without masonry infill in ABAQUS

The finite element model was developed using Abaqus software to simulate the structural behaviour of a reinforced concrete frame with a masonry infill wall based on the experimental study conducted by Seki et al., (2018) as shown in Figure 3.7. The model consisted of a single-bay frame comprising two vertical columns and two horizontal beams, forming an enclosed structural system with an infill wall and another similar Frame without infill.

The columns were modelled as 3D solid elements with cross-sectional dimensions of 250 mm × 250 mm, while the beams were similarly represented as 3D solid elements with dimensions of 250 mm × 300 mm. The reinforcement within the beams and columns was explicitly modelled using 2D wire elements, accurately capturing the longitudinal and transverse steel layout with precise geometric detailing. The masonry infill wall, assumed to behave as a homogeneous material, was modelled as a 3D continuum element of a 115mm thickness, integrated within the frame.

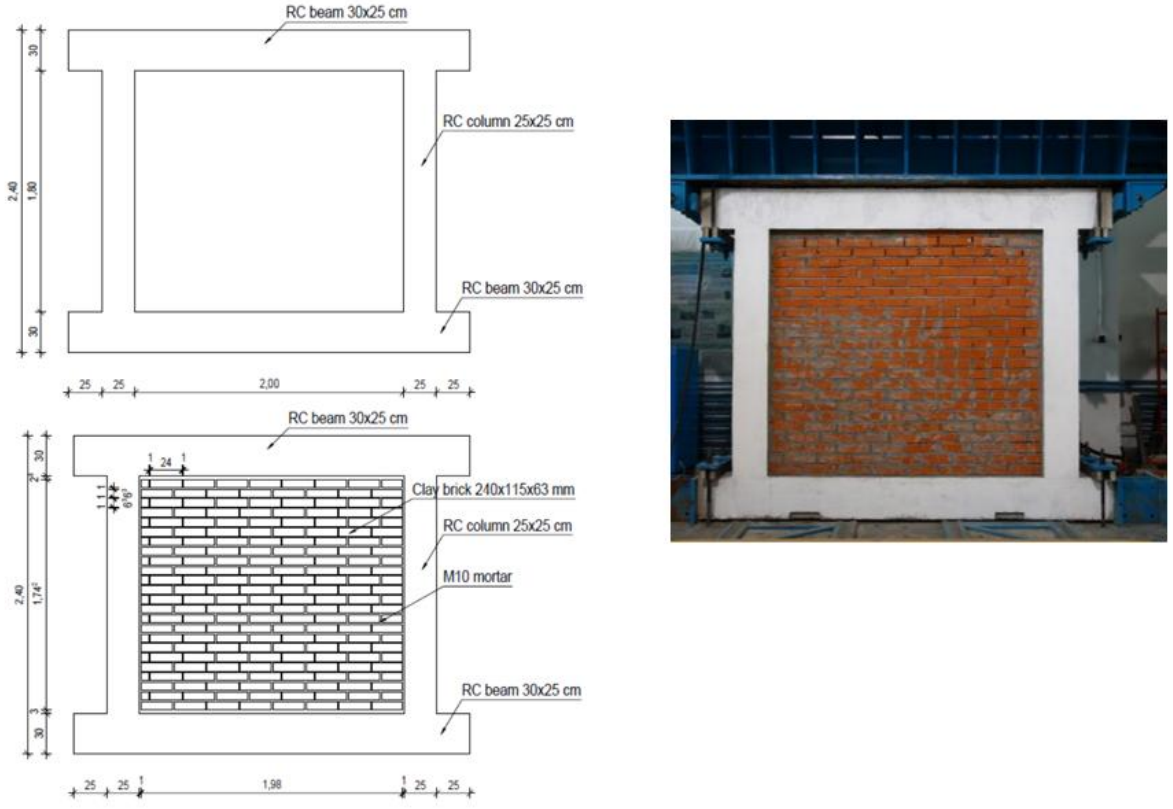

Figure 3.6 RC Frame with and without masonry infill

The material properties were systematically assigned to each component of the finite element model to ensure accurate representation of their mechanical behaviour. The concrete elements, corresponding to compressive strength of 14 MPa, were characterised by their elastic modulus of 28 GPa and Poisson's ratio of 0.18, in accordance with Eurocode 2 specifications. To account for the nonlinear behaviour of concrete under loading, the Concrete Damaged Plasticity (CDP) model was employed, incorporating parameters such as the dilation angle of 31^0. The reinforcing steel was modelled as an elastic-perfectly plastic material with a defined yield strength of 428.61 MPa, ultimate strength of 525.96 MPa, Young's modulus of 200 GPa and a Poisson's ratio of 0.3.

For the masonry infill wall, material properties were derived from the experimental study by Seki et al., (2018), with key parameters, including compressive strength and elastic modulus, summarised in Table 3-3. To accurately simulate the infill's nonlinear response, the Drucker-Prager plasticity criterion was employed, which accounts for its shear failure characteristics. This constitutive model incorporated cohesion, internal friction angle, and dilation behaviour to replicate the infill's in-plane resistance.

Table 3-3 Masonry Material Properties

Material Properties	**Values**
Compressive strength	11.6 MPa
Modulus of Elasticity	6380 MPa
Poisson's Ratio	0.2
Angle of friction	31.79
Flow stress ratio	0.8
Dilation Angle	2.86
Shear strength	0.58 MPa

Following the material property assignments, the individual model components—beams, columns, reinforcement, and masonry infill, were assembled.

A general static step was introduced to simulate the quasi-static response of the structure under applied loads. The step was configured with a maximum allowable increment count of 10,000 to ensure numerical convergence, while an initial time increment of 0.01 was set to facilitate a stable onset of the solution. To maintain computational accuracy, the minimum increment size was restricted to 1×10^{-15}, preventing premature termination due to excessive iteration cuts.

The maximum increment size was capped at 1 to avoid unrealistic load application rates. Boundary conditions were imposed with the base of the frame fully fixed to simulate a rigid foundation connection. Following the experimental loading approach used by Seki et al. (2018), a constant axial load of 350 kN was applied to each column, along with a monotonic lateral displacement of 50 mm, equivalent to 2.5% of the column height in the push direction from the left side. In the finite element model, this axial load was represented as a uniform normal stress of 5.6 N/mm², distributed over the top surface of the upper beam, corresponding to the projected cross-sectional area of the column, as illustrated in Figure 3.8.

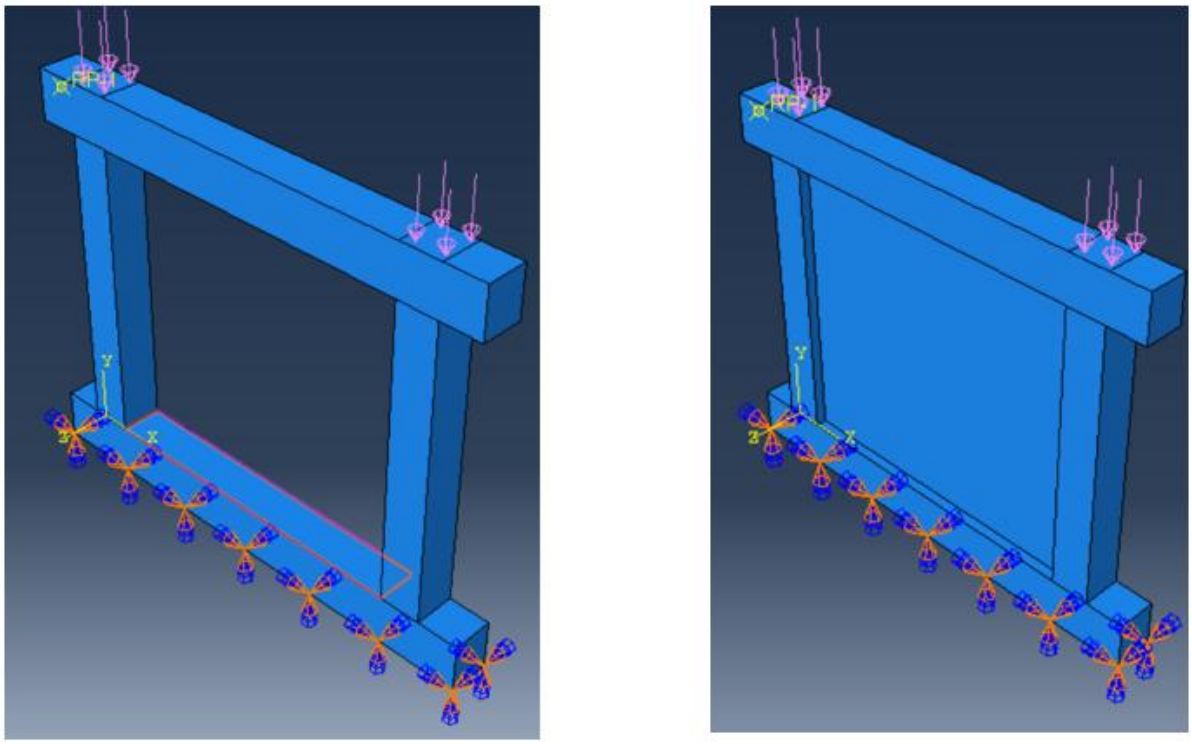

Figure 3.7 Model Boundary Conditions

Interaction properties were carefully defined to model the composite behaviour of the system. The reinforcement bars were embedded within the concrete elements using the *embedded region* constraint, ensuring full bond-slip interaction between the steel and the surrounding concrete. Additionally, a *tie* constraint was applied at the beam-column joints to enforce full kinematic compatibility, simulating rigid connections typical of moment-resisting frames.

For the masonry infill wall, a surface-to-surface interaction was established with the surrounding concrete frame to capture normal and tangential contact behaviour. A *hard contact* formulation governed the normal interaction, preventing penetration between surfaces, while a penalty-based friction model defined the tangential behaviour, accounting for potential sliding and shear transfer. The concrete surfaces were designated as the primary contact

surfaces, and the infill wall surfaces as secondary, ensuring proper load transfer and interaction stresses at the frame-infill interface.

The finite element model was discretised using a structured meshing scheme to ensure computational efficiency while maintaining solution accuracy, as shown in Figure 3.9. The beams, columns, and masonry infill wall were assigned a global seed size of 50 mm, resulting in a balanced mesh density capable of capturing stress gradients and deformation patterns without excessive refinement. For the reinforcement bars, a finer mesh size of 200 mm was employed to accurately model the steel-concrete interaction and localised strain behaviour, particularly in critical regions such as plastic hinges and lap splices.

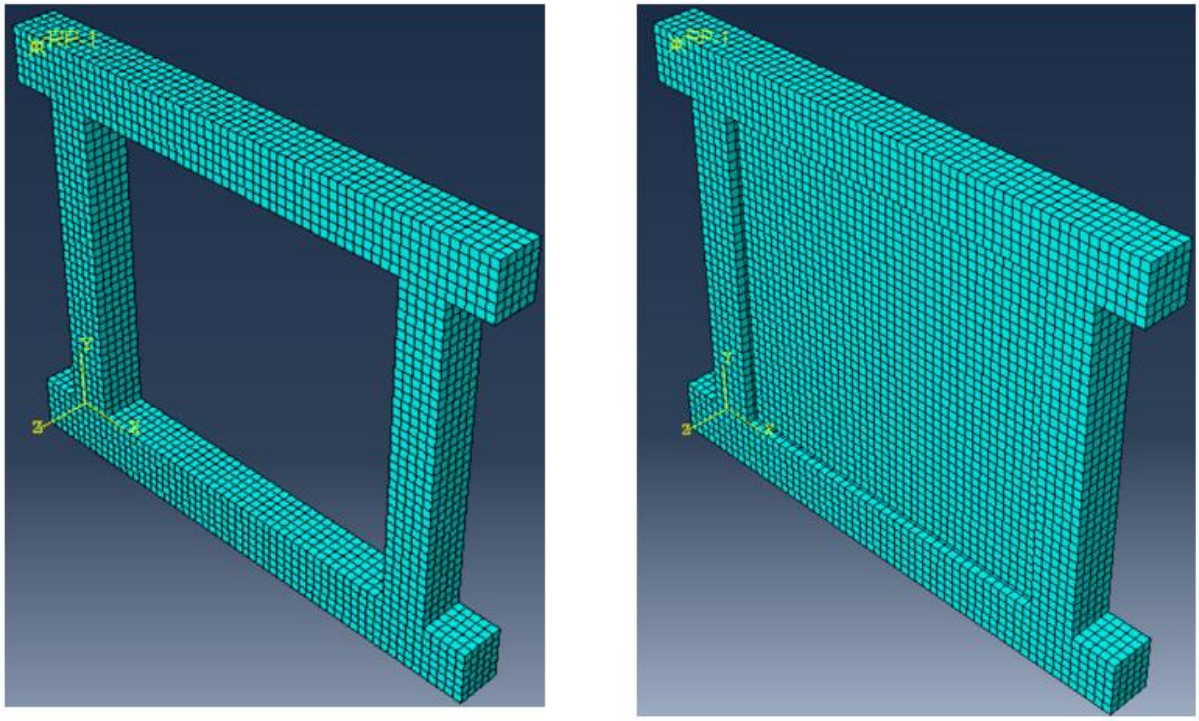

Figure 3.8 Model mesh

Following meshing, a computational job was created within Abaqus/Standard to execute the nonlinear static analysis. Post-processing of the results was then conducted to evaluate structural performance, including stress distribution in both the reinforced concrete frame and masonry infill under the prescribed lateral displacement.

3.6 Developing a Diagonal Strut Model

Due to the high computational power required to accurately model a single reinforced concrete frame with masonry infill in finite element analysis, extending such detailed modelling to more complex and larger structures, such as multi-story buildings up to 10 stories, becomes highly inefficient, particularly for global seismic analysis. This level of complexity not only increases

analysis time but also significantly hinders iterative design processes. As a result, an equivalent diagonal strut was used to represent the behaviour of masonry infill walls, which was done using the ETABS software.

The procedure involved modelling a single frame in ETABS, similar to the one previously analysed using the Finite Element Method. The beam and column dimensions, as well as the material properties, were kept identical to ensure consistency between the two models. The masonry infill was represented using an equivalent diagonal strut, with its width calculated from Equations 3-10 to 3-13 provided in Section 3.4.2. This calculation yielded a strut width of 290 mm, and the same material properties as those in the experimental study were assigned to the strut to maintain uniformity. The Frame was modelled in ETABS as shown in Figure 3.10.

To simulate nonlinear behaviour, plastic hinges were strategically placed on the structural elements. For the columns and beams, these hinges were applied at relative distances of 0 and 1, corresponding to their ends, where plastic deformation was most likely to occur under lateral loading. In contrast, the diagonal strut was assigned a plastic hinge at its mid-length, represented by a relative distance of 0.5, to account for potential yielding or buckling at the centre of the strut.

Once the model was fully defined, a 350kN axial load was applied to each column, and a pushover analysis was conducted to evaluate the frame's performance under progressively increasing lateral loads until failure. A controlled displacement of 50mm was used to match the one in the FEM model. The results were then analysed to assess the frame's seismic performance and compare it with the FEM-based findings.

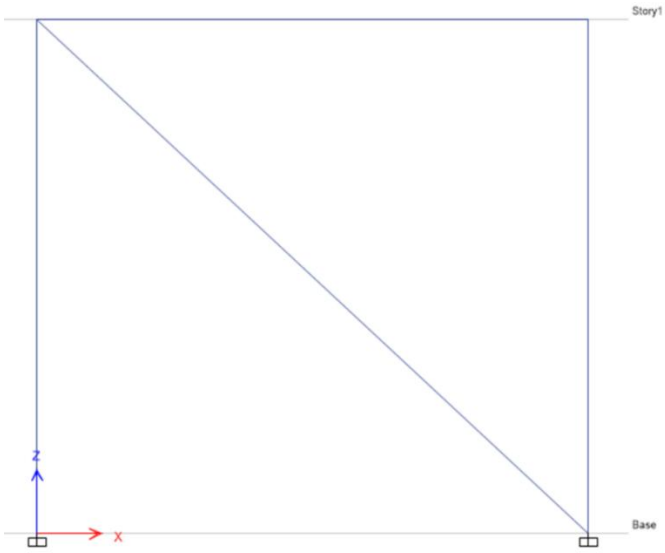

Figure 3.9 Single Frame ETABS model

3.7 A Brief on the experiment used to validate numerical models in ETABS

The Validation was done based on an experimental study by Negro & Verzeletti, (1996) that carried out a seismic analysis on a four-storey frame, with and without masonry infill, as shown in Figure 3.11.

Figure 3.10 Experimental design of frame structure, with and without masonry infill

The first test was conducted on the bare frame. The project was conducted within the framework of the European Association of Structural Mechanics Laboratories (EASML) and aimed to evaluate the suitability of damage indicators for use in the calibration of Eurocode 8. A pseudodynamic test was conducted using an artificially generated earthquake derived from the 1976 Friuli earthquake. A second experimental programme was conducted as part of the work of the Network Prenormative Research in support of Eurocode 8, to study the influence of masonry infill panels on the global behaviour of the frame. The test was performed by infilling the two external frames with hollow brick masonry in all four storeys, hence a uniform infill distribution. The input signal was the same as in the tests on the bare frame.

3.7.1 ETABS Modelling

Table 3-4 Properties of Reinforced Concrete Frame

Building Height	1st Storey	2nd, 3rd and 4th Storey
Storey height	3.5m	3m
Surrounding Columns	400mm × 400mm	
Interior Column	450mm × 450mm	

Building Height	1st Storey	2nd, 3rd and 4th Storey
Beam	300mm × 450mm	
Slab	150 mm	
Floor finish	2kN/m^2	
Live load	2kN/m^2	
Concrete grade	C25/30	
Steel yield strength	500MPa	
Local soil conditions	Soil Type B-Medium	
Damping ratio	5%	

Table 3-5 Masonry Infill properties

Masonry type	Construction Block
Wall thickness (t)	112mm
Compressive strength of Block/ Brick (f_b)	7MPa
Compressive strength of Mortar (f_{m0})	5MPa

To validate the ETABS model using the experimental study, a systematic approach was adopted to ensure that the numerical results closely matched the experimental findings. First, the Columns, Beams and slabs were modelled with their respective geometrical properties to make up the bare RC frame as shown in Table 3-4. They were then assigned their material properties and loading conditions as in the experimental study. For the frame with infill, masonry was modelled by representing it as equivalent diagonal struts using the set of Equations 3-10 to 3-13, listed in section 3.4.2 and using the masonry properties from the experimental study shown in Table 3-5. The diagonal strut width was achieved for the different frames as shown in Appendix II. The models generated are shown in Figure 3.12.

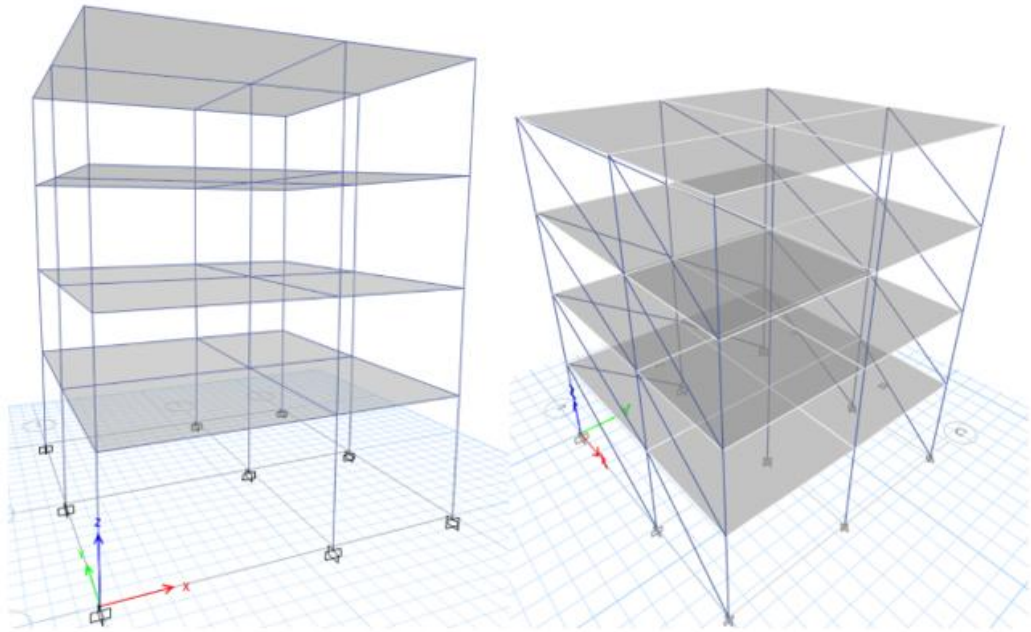

Figure 3.11 Representative Models in ETABS

Hinges were then assigned. They were first assigned to the beams by selecting all the beams in the model, then going to *Assign>Frames and Hinges*. In the Frame Assignment - Hinges window, all the parameters were selected very carefully with reference to ASCE guides. Then the relative distance was chosen, which varies from 0 to 1, 0 being one end and 1 being the other end of the frame. Relative distance specifies the location where the hinge will be formed. The hinges are likely to form where the bending moment is maximum. So, two hinges were assigned to the frame. First, 0 was put for relative distance and add was clicked as shown in Figure 3.13. This displayed a new dialogue box as shown in Figure 3.14.

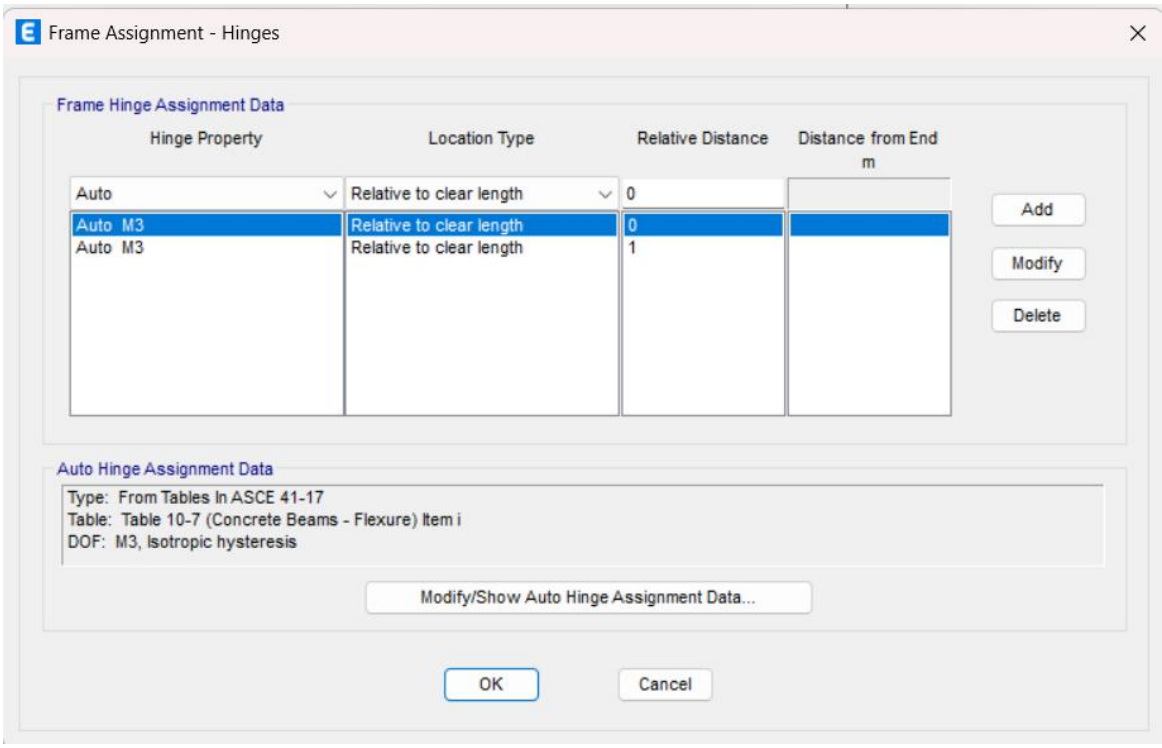

Figure 3.12 Frame assignment- Hinges window

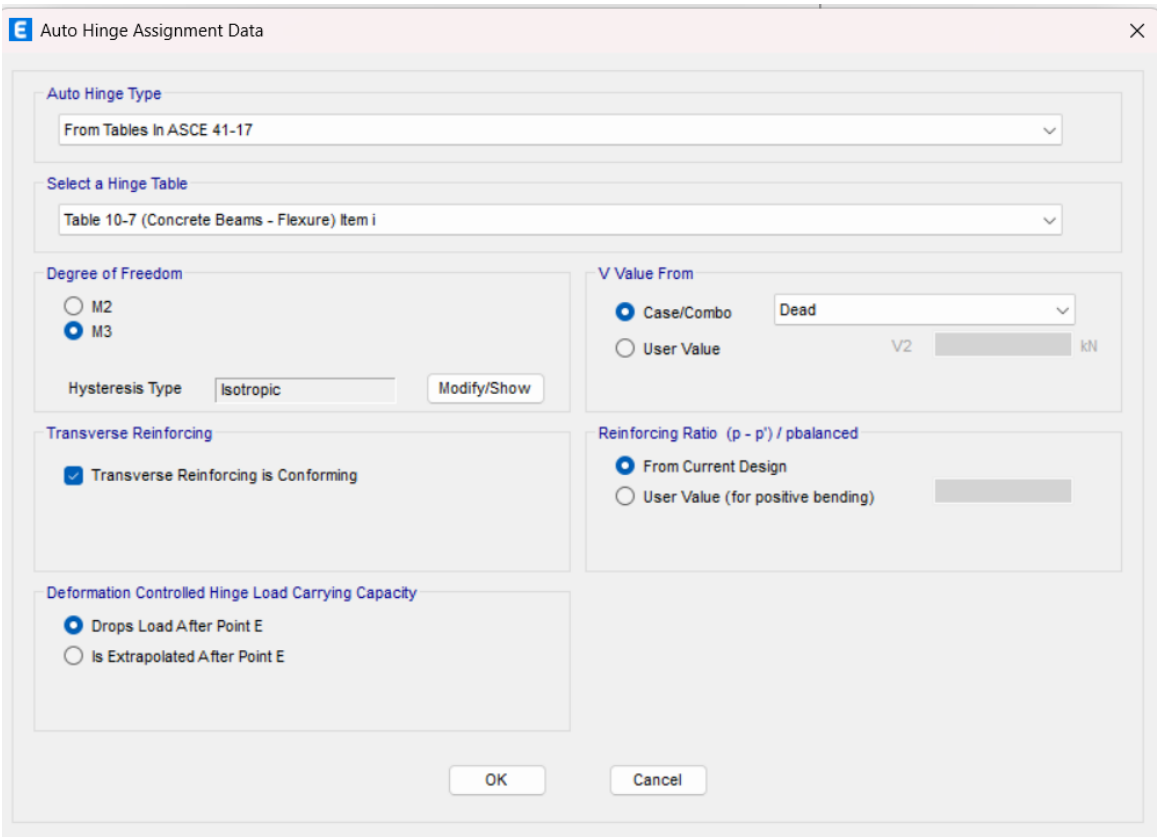

Figure 3.13 Auto Hinge Assignment Data for Beams

Here, the hinge table was selected as Table 10-7, Concrete beams. This is from ASCE 41-17. The degree of freedom was M3 for beams, since M3 is the major bending axis in ETABS. The reinforcing ratio was selected from the current design. The V value shown in Figure 3.9 is the design shear force that is developed in beams during the formation of a plastic hinge. The load combination was chosen, and ETABS took the shear force from that combination. To assign another hinge at the other end, 1 was selected as the relative distance, and the process was repeated. The columns were then selected, and the above process was repeated, but this time, Concrete columns were selected as the hinge table. The degree of freedom was selected where P-M2-M3 was the general type of hinge. P is the compression, and M2 and M3 are moments about the 2nd and 3rd axes in the columns, as shown in Figure 3.14.

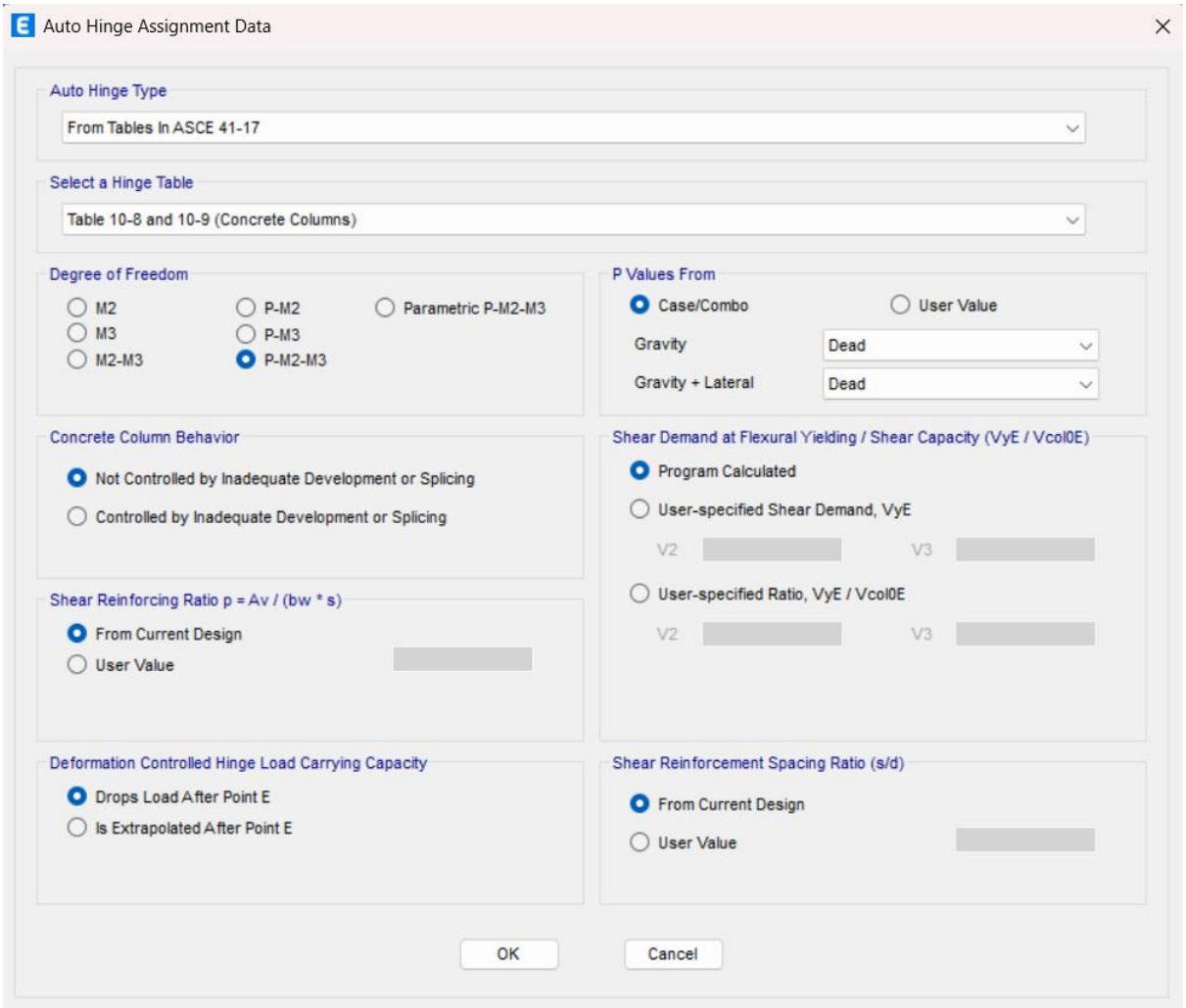

Figure 3.14 Auto Hinge Assignment Data for Columns

For the masonry infill, a new hinge property type has to first be defined by going to define>section properties>Frame/wall Non-linear Hinges>add new property. From there, select Force controlled and axial P, as shown in Figure 3.11.

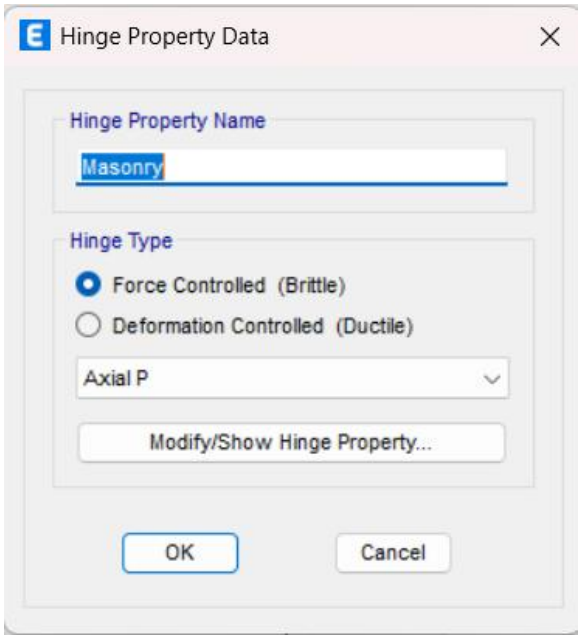

Figure 3.15 Hinge Property Data Window

The diagonal struts are selected, and at the Frame assignment, instead of Auto, the hinge property is masonry and the relative distance is 0.5 as shown in Figure 3-12.

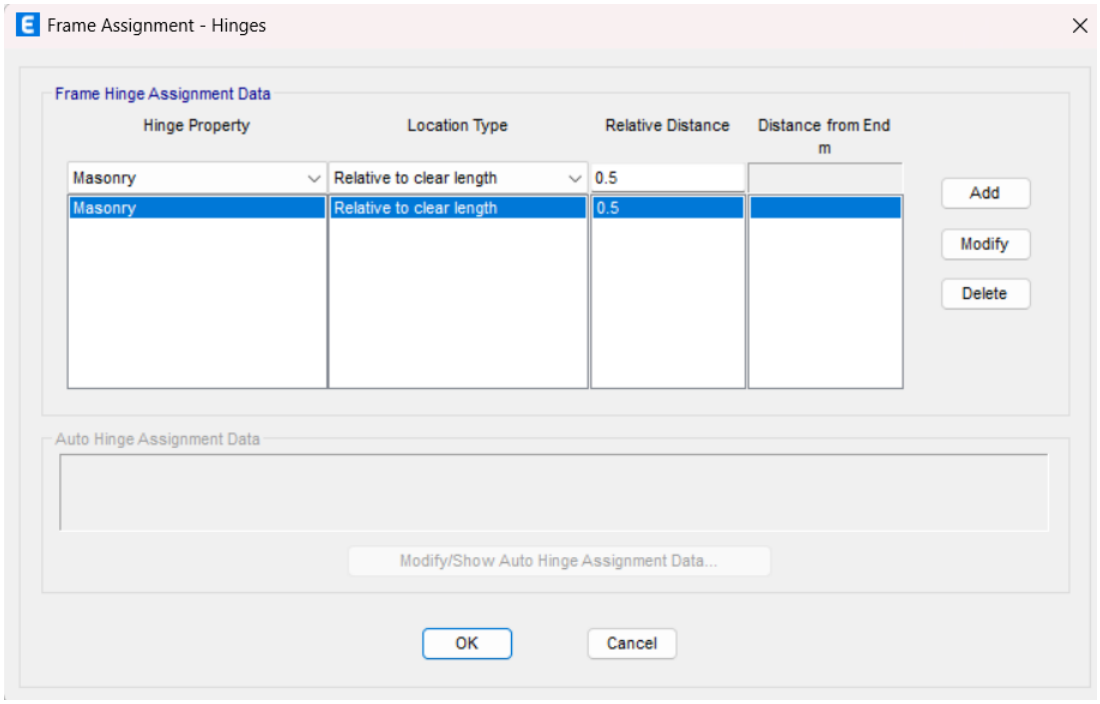

Figure 3.16 Hinges Assignment Window for Masonry

3.7.2 Pushover analysis

In the nonlinear static analysis setup, a new load case was created by navigating to *Define* > *Load Cases* and selecting *Add New Case*. The load case type was specified as *Nonlinear Static*,

and for simplicity, the initial conditions were set to *continue from state at End of non-linear case* as shown in Figure 3.13. Existing dead and live loads were selected based on the prior definition of a separate nonlinear load case incorporating these loads.

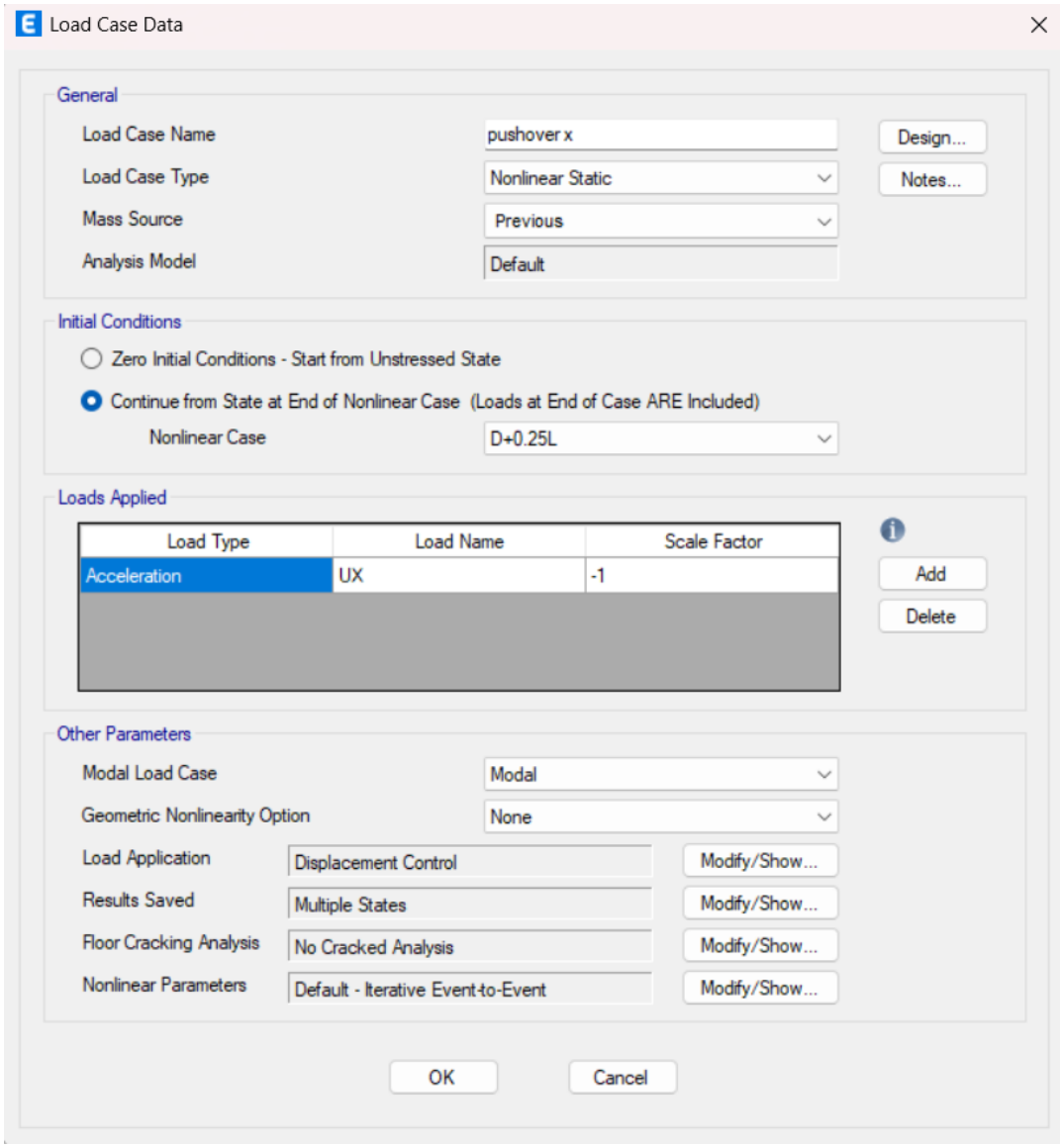

Figure 3.17 Pushover Load case data window

Within the *Loads Applied* section, *Acceleration* was chosen as the load type. Alternatively, *Load Pattern* could have been selected if the analysis required predefined loads with appropriate scale factors. For structures where modal contributions are significant, such as medium- to high-rise buildings, a multi-mode pushover analysis might be necessary. In this case, a scale factor of -1 was applied to ensure the base shear curve would appear in the positive quadrant. The *Modify/Show* option was then accessed to configure the load application control. *Displacement Control* was selected, with a target monitored displacement of *260 mm* specified as the stopping criterion for the analysis. The monitored displacement was

assigned to a joint at the top story, ensuring the analysis would terminate once this displacement threshold was reached, as shown in Figure 3.18. By default, ETABS saves only the final results; however, to generate the pushover curve, the output settings were adjusted to retain *Multiple States*. This completed the definition of the nonlinear load case.

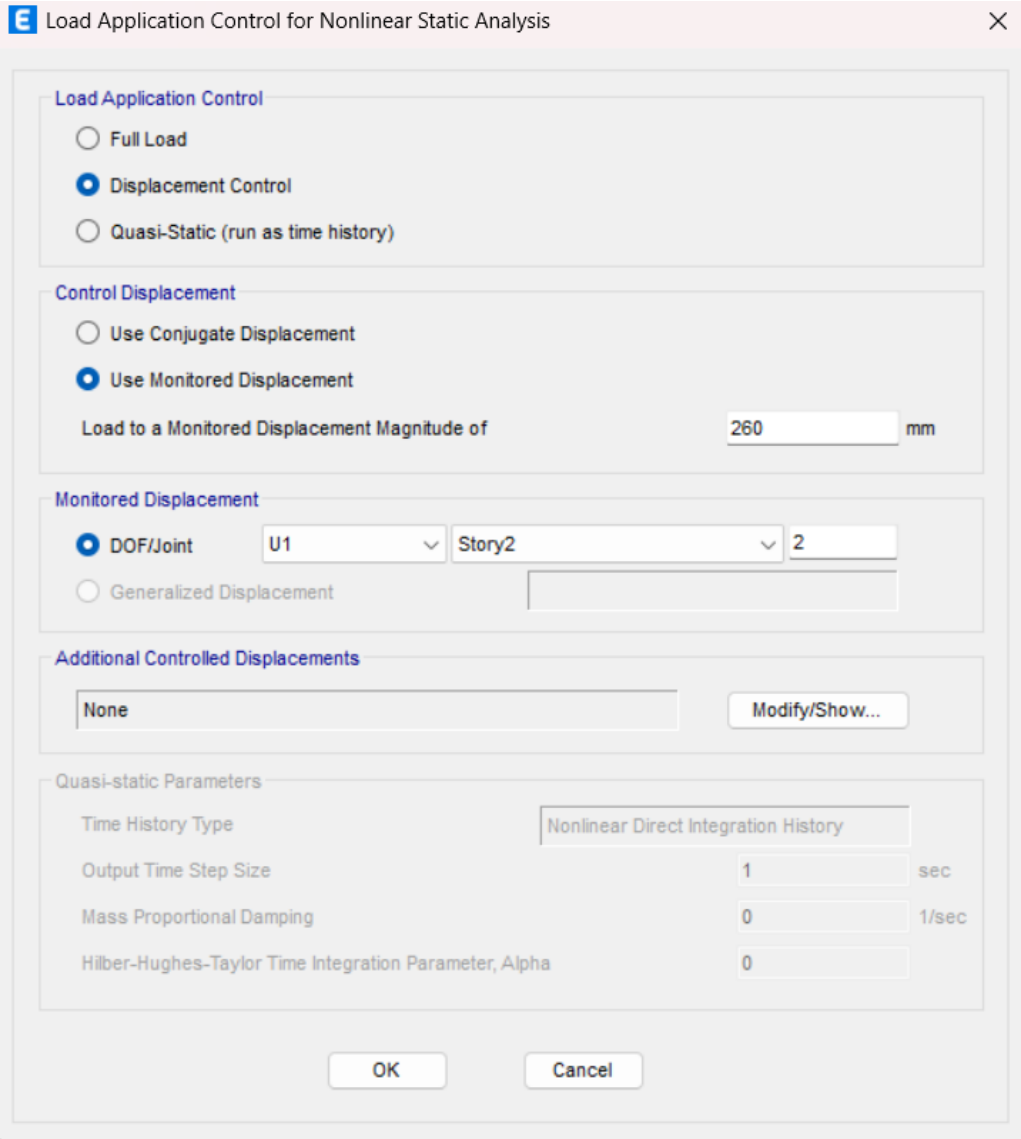

Figure 3.18 Load Application Control for Nonlinear Static Analysis

The pseudodynamic test input, based on the Friuli earthquake record scaled to 0.45 g, was applied to the model, and nonlinear static pushover analysis was performed to simulate the seismic response. The seismic demand of Friuli was also implemented by inputting its spectral acceleration at 1 second and short periods and generating its response spectrum as shown in Figure 3.20.

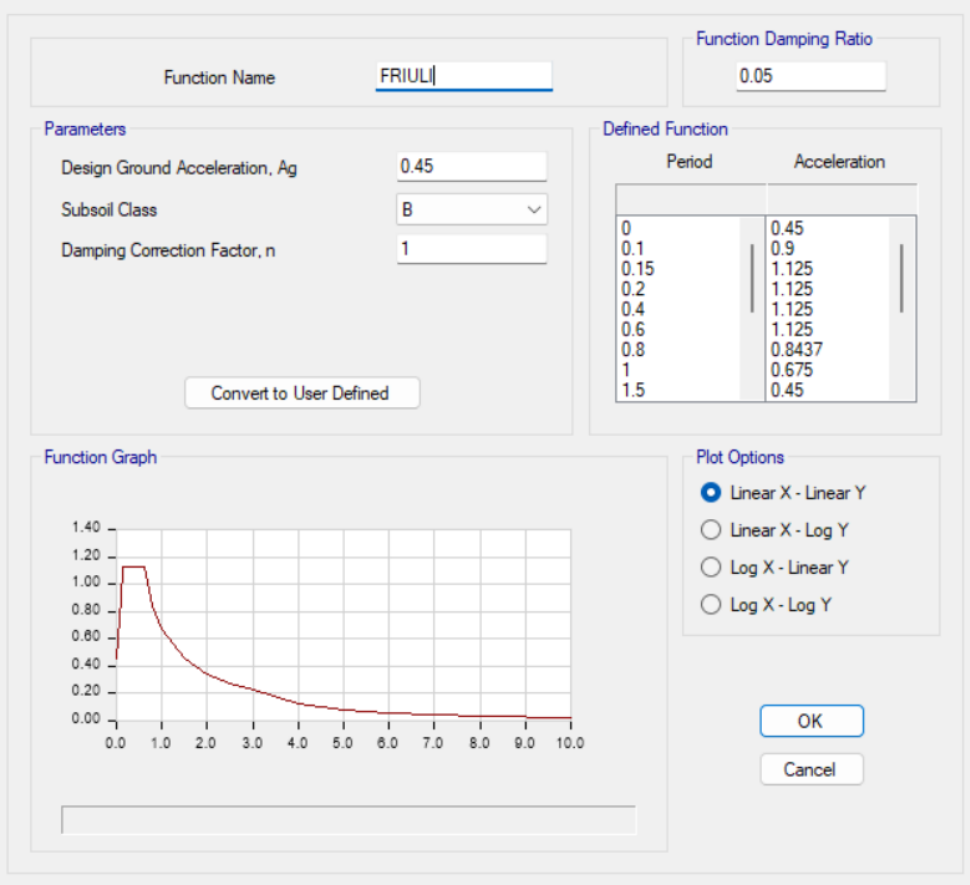

Figure 3.19 Friuli response spectrum

After running the analysis, the static pushover curve was generated by navigating to *Display* > *Static Pushover Curve* and selecting the plot type as FEMA 440 EL as shown in Figure 3.21. The load case was set to the predefined nonlinear load case, which, in this instance, was Pushover x, representing the nonlinear load case in the x-direction. The spectrum source, which was the Friuli Response Spectrum Function, was selected. A scale factor of 9810 was applied to the response spectrum function to account for the acceleration due to gravity (g), as spectral values are provided relative to g. The performance point was observed at the 10th step of the pushover analysis, suggesting that ten stages of plastic deformation would occur during the seismic event. To visualise the seismic response of the structure in terms of Displacement, Drift, and Base shear, the deformed shape was examined at the 10th step.

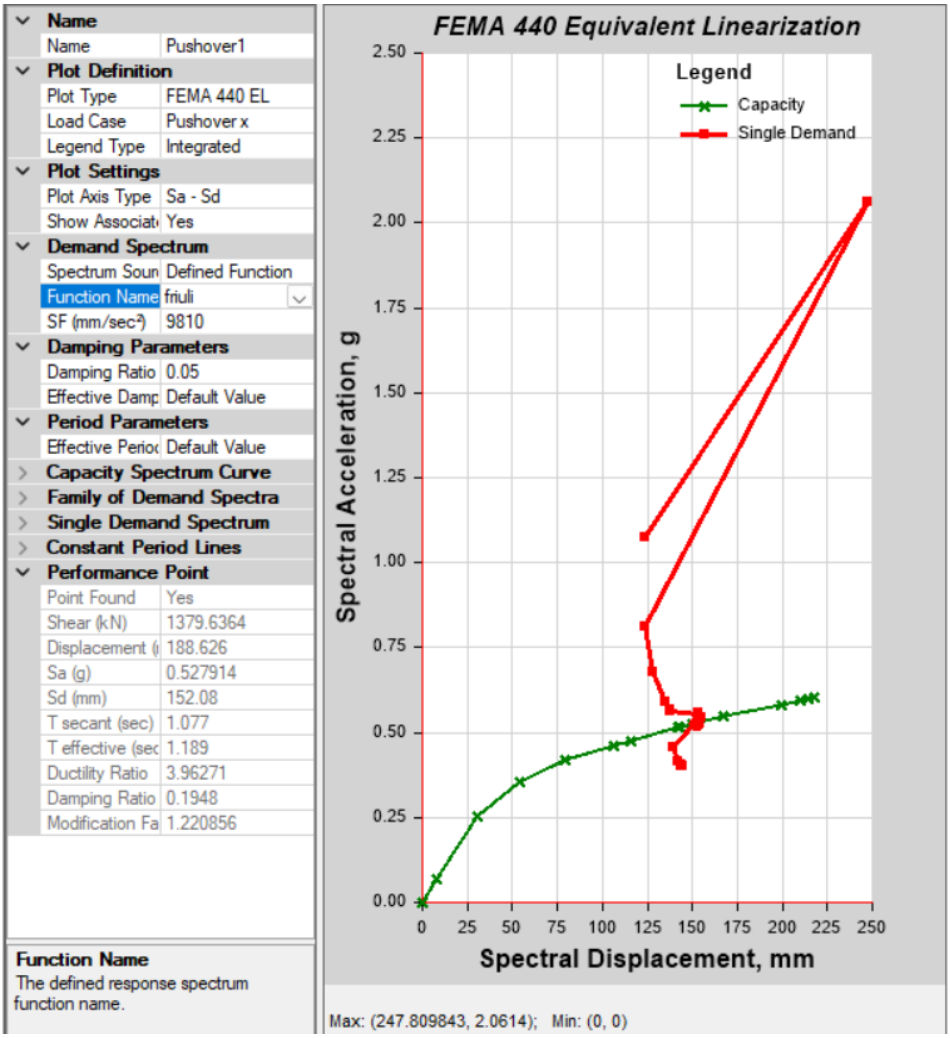

Figure 3.20 FEMA equivalent linearization

3.8 Parametric analysis

After validation, two types of models were generated, one with a bare RC frame and another with masonry infill. The different structures were done for each of the models, having 2, 5, and 10 stories with a similar configuration as the validated model. The masonry infill model considered different masonry types, like masonry made of clay bricks and that of Concrete blocks with their respective mechanical properties.

The following are the parameters considered for the reinforced concrete frame as shown in Table 3-6. The column and Beam sizes were selected based on preliminary design and common practice in Uganda to ensure a realistic representation of typical RC frame structures, while the material properties reflect locally available construction materials. The importance factor 1.5 was chosen to account for high occupancy buildings, and a live load of $2kN/m^2$ represents typical residential or office loading conditions in Uganda, as indicated in the Uganda National Building Code. These values were used to maintain consistency with regional construction

standards while ensuring the models accurately simulate real-world behaviour under seismic loads.

Table 3-6 Reinforced Concrete Frame Parameters

Building Height	G+1	G+4	G+9
Storey height	3m	3m	3m
Column	200mm × 200mm	300mm × 300mm	400mm × 400mm
Beam	200mm × 450mm	200mm × 450mm	300 × 450mm
Slab	150 mm		
Floor finish	2kN/m^2		
Live load	2kN/m^2		
Concrete grade	C25/30		
Steel yield strength	460MPa		
Zone	1		
Importance factor	1.5		
Local soil conditions	type II-Medium		
Damping ratio	5%		

3.8.1 Masonry properties

To determine the representative compressive strength values for both concrete blocks and clay bricks, a systematic laboratory testing procedure was followed. First, 10 samples were collected from different sites, consisting of 5 concrete blocks and 5 clay bricks. Each sample was then weighed and measured to determine its dimensions (length, width, and height) as shown in Figure 3.22, ensuring accurate calculations of cross-sectional area for stress determination. The compressive strength test was conducted using a universal compression testing machine, where each specimen was placed between two parallel steel plates and subjected to a gradually increasing axial load until failure, as shown in Figures 3.23 and 3.24. The maximum load at failure was recorded, and the compressive strength was calculated by dividing this load by the cross-sectional area of the specimen, as shown in Appendix I. For each material type, the individual compressive strengths were analysed statistically to determine the mean value. The final representative compressive strength values for concrete blocks and clay bricks were

reported as the mean values of the five tested samples for each material, as shown in Table 3-7.

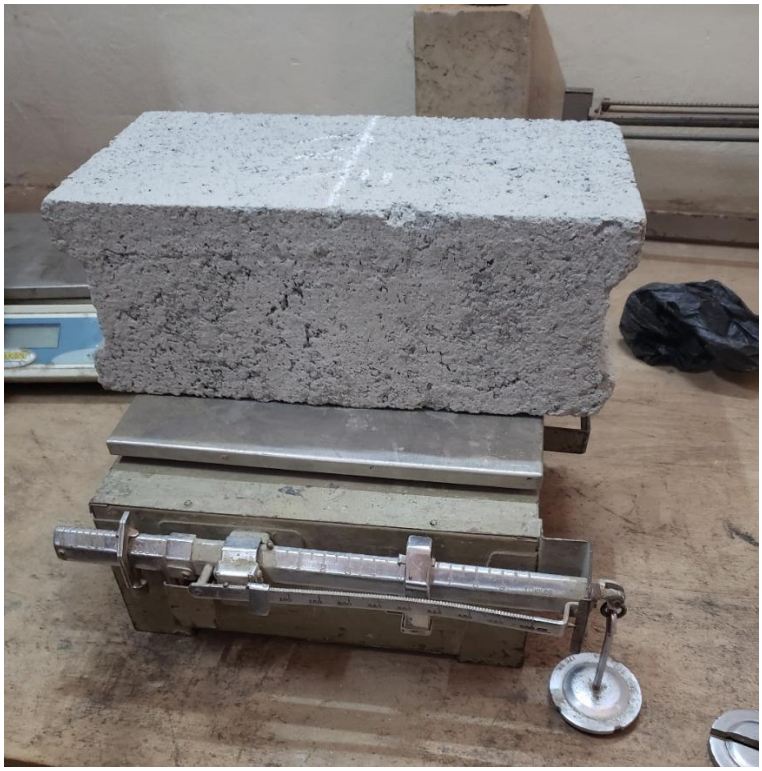

Figure 3.21 Weighing concrete Block sample

Figure 3.22 Compressive test on concrete Block sample

Figure 3.23 Compressive test on clay brick sample

Table 3-7 Masonry Infill properties

Masonry type	Solid Concrete Block	Clay Brick
Wall thickness (t)	150mm	100mm
Compressive strength of Block/ Brick (f_b)	3.47 Mpa	2.56 Mpa
Compressive strength of Mortar (f_{m0})	6.5 MPa	

The mortar compressive strength value was obtained from the Uganda National Building Code, which provides standardised strength specifications for various mortar mix ratios. For this study, a 1:3 cement-sand mix ratio was selected, and the compressive strength value was based on preliminary laboratory tests as documented in the code, ensuring a controlled and reliable reference. The UNBC distinguishes between lab-tested mortar samples and site samples, as shown in Part IV of the code as shown in Appendix I. By adopting the lab-derived compressive strength, the analysis benefits from higher consistency and repeatability, as these values are determined through standardised compression tests on properly cured mortar cubes at 28 days.

This approach minimises uncertainties associated with field conditions, providing a robust baseline for structural assessment.

3.8.2 Modelling and analysis of RC frame structures at different heights

The reinforced concrete frames were modelled in ETABS using the parameters as shown in Table 3-4. The Geometrical properties of the columns and beams were selected to account for the respective heights of the different structures.

For the frame with infill, the masonry was modelled as an equivalent diagonal strut using the parameters as shown in Table 3-5. This was done based on the set of equations 1-4 listed in section 3.4. The respective width of the struts is represented in Appendix II. The models were then finally developed as shown in Figures A.1 to A.3, as shown in Appendix IV. This systematic approach ensured that both the bare frame and infill-enhanced structures were accurately captured in the analysis. The plastic Hinges were then applied in the columns, beams and struts.

Pushover analysis was used to analyse the models. The Seismic demand of Fort Portal was then defined by inputting the design response spectrum of Fort Portal as shown in Figure 3.27. The performance point was obtained from the FEMA 440 Equivalent Linearization, giving the required step for the respective models. From here, the seismic performance of the models was determined, which included storey displacement, base shear and storey drift.

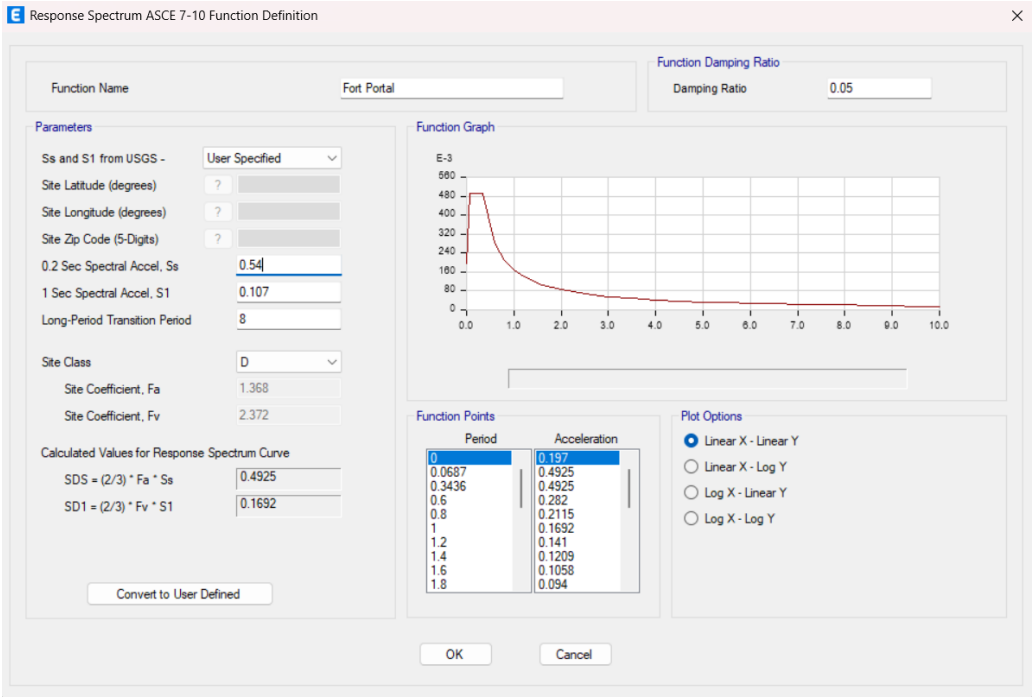

Figure 3.24 Fort Portal response spectrum input in ETABS

CHAPTER 4: RESULTS

4.1 Design response spectrum of Fort Portal

The set of Equations 3-1 to 3.9 listed in section 3.2.1 were put in Excel to come up with input values as shown in Table 4-1, and subsequently, the design response spectrum of Fort Poral as shown in Figure 4-1. The coordinates of the spectrum are shown in Appendix III. This was used to represent the seismic demand of Uganda.

Table 4-1 Response spectrum input values

Parameter	Value	Description
S_S	0.54 g	Spectral acceleration at short periods
S_1	0.107 g	Spectral acceleration at 1s
F_a	1.368	Short-period site coefficient (ASCE 7-22)
F_v	2.372	Long-period site coefficient (ASCE 7-22)
S_{MS}	0.739 g	Site-adjusted spectral acceleration at short-period
S_{M1}	0.254 g	Site-adjusted spectral acceleration at 1 second
S_{DS}	0.493 g	Design spectral acceleration at short periods
S_{D1}	0.169 g	Design spectral acceleration at 1 second
T_S	0.343 s	Transition period
T_L	8 s	Long-period transition (ASCE 7-22)

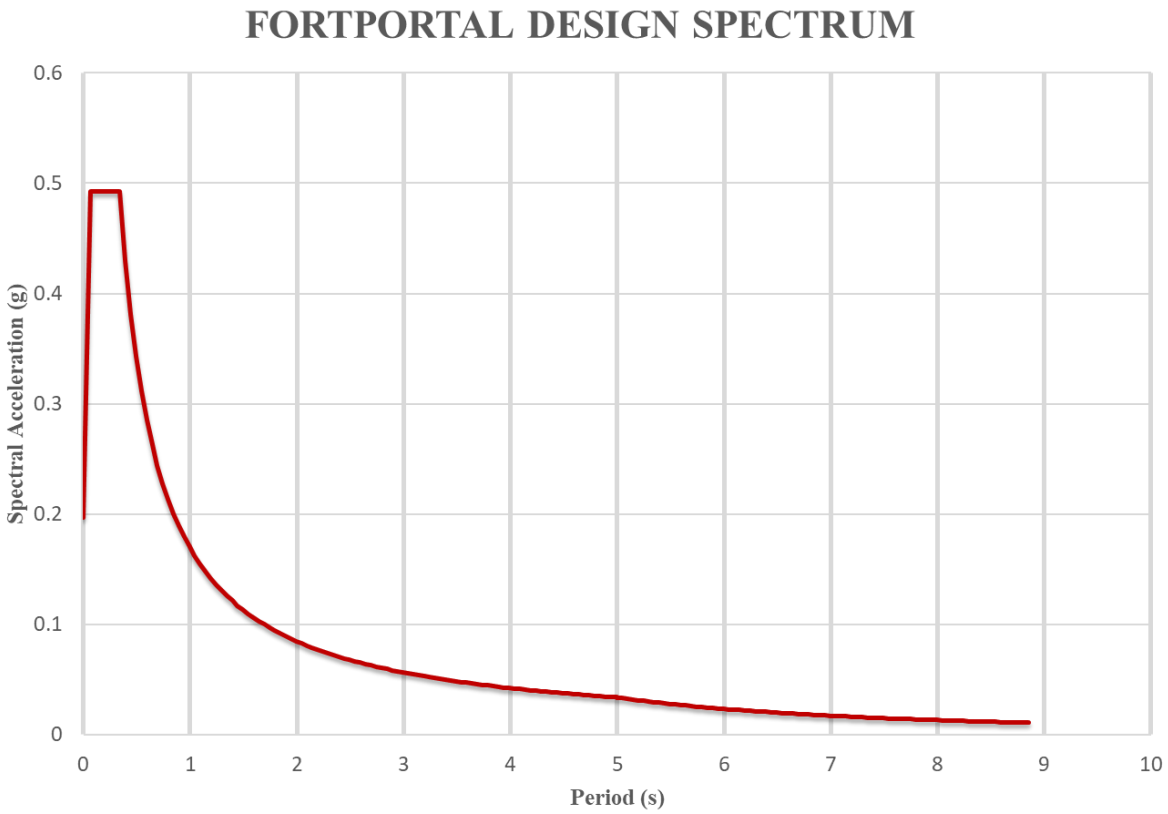

Figure 4.1 Fort Portal Design spectrum

4.2 FE model results

4.2.1 Bare RC frame

The von Mises stress results from the pushover analysis of the bare RC frame reveal a stress distribution ranging from 4.467e-05 MPa to 12.3 MPa, as shown in Figure 4.2. The maximum stress concentration occurs at the beam-column joints. The stress values are shown to decrease progressively toward the mid-spans of beams and columns. The high von Mises stresses of 12.3 MPa are located at the lower right joint, which may approach or exceed the cracking

strength of concrete and indicate potential yielding of reinforcement.

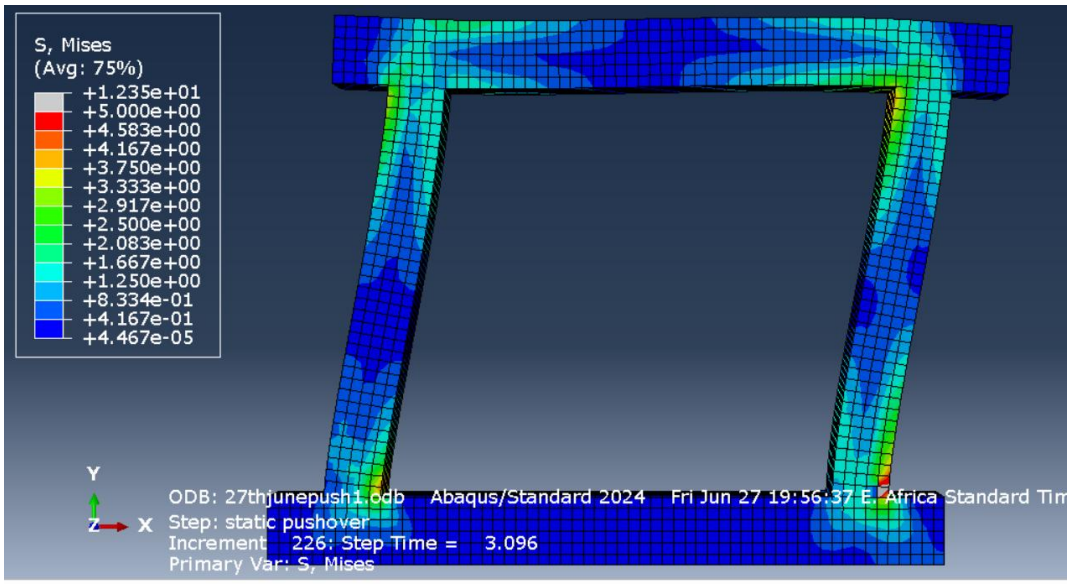

Figure 4.2 Stress contours of Bare RC frame

4.2.2 RC frame with masonry infill

The results for the RC frame with infill exhibit the emergence of diagonal stress contours within the masonry infill, which visually manifest as bands of elevated stress extending from the upper corners to the lower opposing corners of the panel. The stress ranges from 2.001e-05 MPa to 5.14 MPa, with the maximum stress localised at regions of high geometric or material discontinuity, such as the beam-column joints and the corners of masonry infill panels, as shown in Figure 4.3. The corners along the direction of the diagonal strut remained in contact with the RC frame, while the opposite corners exhibited separation. The analysis step time of 1.299 at increment 283 highlights the computational effort required to resolve the nonlinear interactions between the infill and frame.

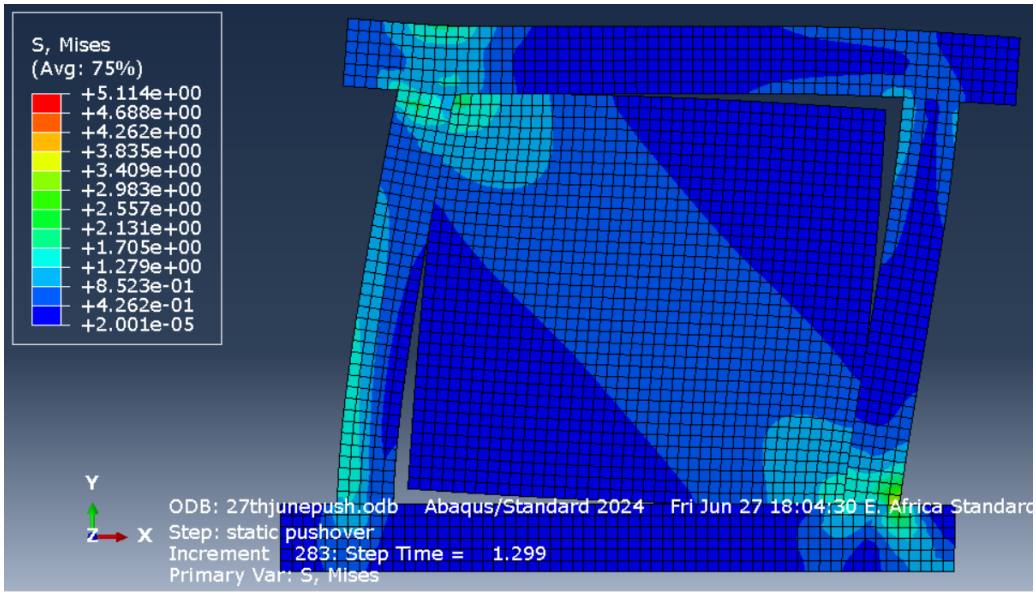

Figure 4.3 Stress contours of RC frame with infill

4.2.3 Validation of FE model

The validation of the finite element models was conducted by comparing the lateral strength versus drift relationships obtained from the numerical simulations with those derived from the experimental study. As illustrated in Figure 4.4, the response and overall behaviour of the FEM closely align with the experimental results, demonstrating consistent load-carrying capacity, stiffness degradation, and energy dissipation characteristics across varying drift levels. The close agreement between the numerical and experimental curves in terms of peak strength, post-yield behaviour, and failure mechanisms confirms the accuracy and reliability of the finite element models in replicating the structural response observed in the physical tests. This correlation validates the adopted modelling assumptions, material properties, and boundary conditions, ensuring that the FEM can be confidently utilised for further parametric studies and performance evaluations.

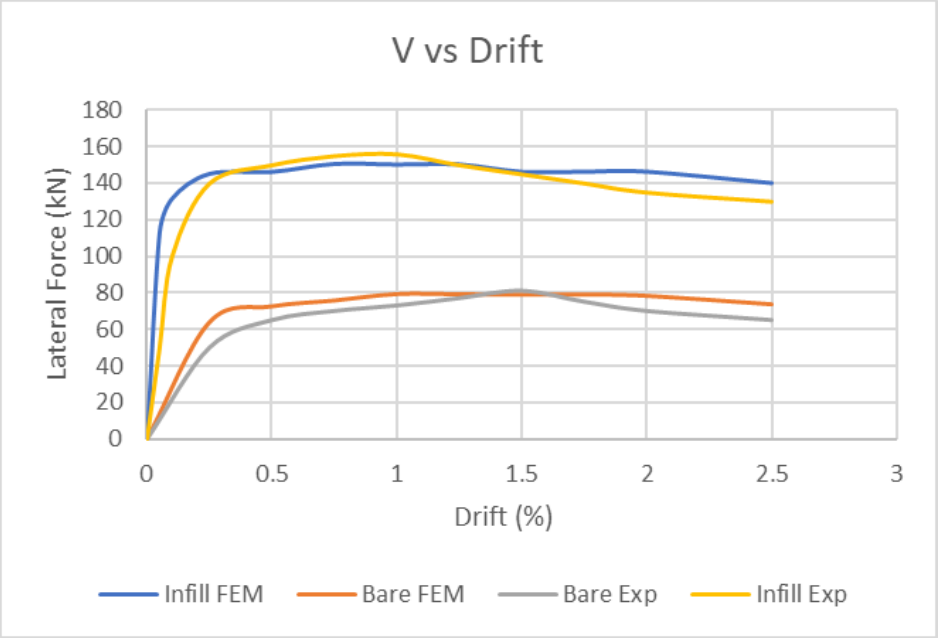

Figure 4.4 Relationship of lateral strength and story drift of bare frame and masonry-infilled RC frame for FE model and Experimental study

4.2.4 Validation of Diagonal Strut

The validation of the ETABS model, incorporating the diagonal strut approach for masonry infill representation, was performed by comparing its lateral strength versus drift relationship with those of both finite element models and experimental test results. As depicted in Figure 4.5, the response of the ETABS model exhibits strong agreement with both the detailed FE simulations and the experimental data, particularly in terms of initial stiffness, peak strength, and post-yield behaviour. The close correlation among the three curves confirms that the simplified diagonal strut method effectively captures the influence of masonry infill panels on the seismic response of the reinforced concrete frame. This validation demonstrates that, despite simplifying the infill as an equivalent diagonal strut, the model reliably predicts key structural characteristics, including stiffness contribution, strength enhancement, and failure progression under lateral loading. Consequently, the ETABS model can be confidently employed for seismic performance assessments of infilled RC frames, providing a practical yet accurate analytical tool.

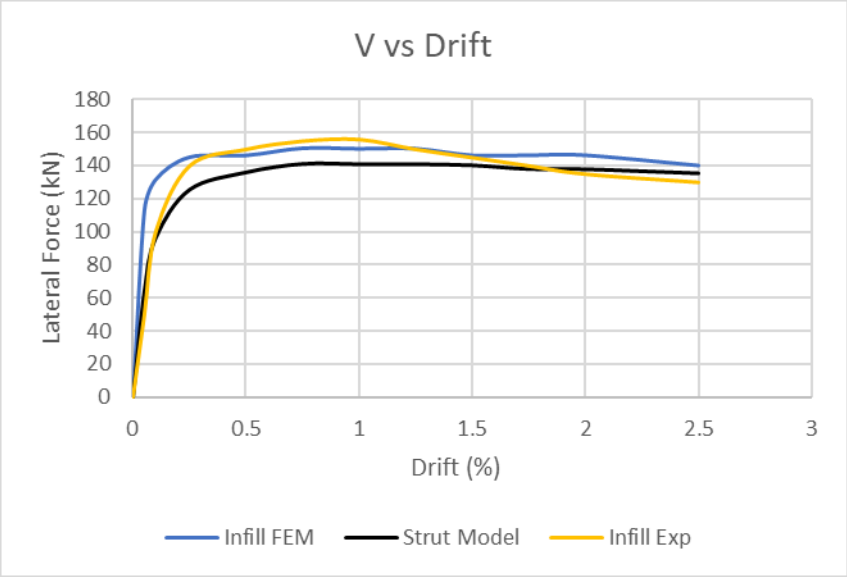

Figure 4.5 Relationship of lateral strength and story drift of the Diagonal strut model, FE model and experimental study

4.3 Validation of Global Numerical Models

To validate the numerical model in ETABS, a detailed comparison was conducted between the experimental results from Negro and Verzeletti (1996) and the simulated outputs for both the bare frame and the masonry-infilled frame. The validation process ensured that the model accurately replicated the experimental behaviour, with all key response parameters, displacement, inter-story drift, and base shear falling within a 5% margin of difference. The results were systematically presented in Table 4-2, listing the experimental values, ETABS model outputs, and their corresponding percentage differences for each parameter. For instance, the bare frame's maximum top displacement in the experiment was 210 mm, while the ETABS model predicted 209.7 mm, resulting in a 0.14% difference. Similarly, the base shear for the uniformly infilled frame was 2.1 MN in the experiment and 2.177 MN in the model, showing only a 3.67% deviation. These minor deviations confirmed the model's reliability.

Table 4-2 Comparison of Experimental and modal results

Structure	Max. Displacement (mm)		Max. Drift (%)		Max. Base shear (kN)	
	Experiment	**Model**	**Experiment**	**Model**	**Experiment**	**Model**
Bare Frame	210	209.7	2.4	2.47	1450	1479
% Difference	0.14%		2.9%		2%	

Structure	Max. Displacement (mm)		Max. Drift (%)		Max. Base shear (kN)	
	Experiment	**Model**	**Experiment**	**Model**	**Experiment**	**Model**
With infill	80	82.2	1.1	1.13	2100	2177
% Difference	2.75%		2.6%		3.67%	

To further illustrate the alignment between experimental and numerical results, graphical representations were generated in Figure 4.2, plotting storey-wise displacement and drift profiles for both configurations. The graphs demonstrated a close match between the curves, with the model accurately capturing the displacement patterns and drift distribution across each storey. For example, the bare frame's experimental drift peaked at 2.4% in the first storey, while the model predicted 2.47%, reinforcing the accuracy of the numerical simulation. The infilled frame's drift reduction from 2.4% to 1.1% was also well-replicated, with the model showing a 1.13% drift, further validating the equivalent strut approach. These visual and tabular comparisons provided a comprehensive verification of the model's accuracy, ensuring its suitability for subsequent parametric studies on the numerical models.

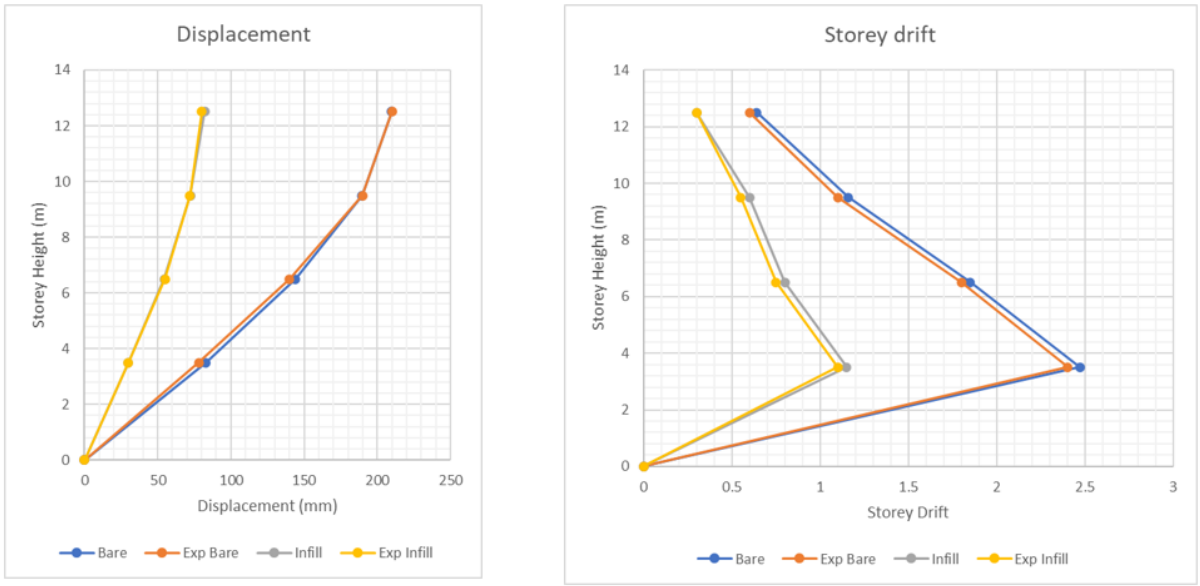

Figure 4.6 Graphical representation comparing experimental and validated results of Storey displacement and Storey Drift

4.4 Numerical model results

4.4.1 Displacement

Figure 4.7 shows the storey Displacement on the 2-storey structure after the pushover analysis, considering the three models of Bare frame, concrete block infill, and clay infill, respectively. The bare frame exhibited the highest displacement at all storeys, while both infilled frames

demonstrated reduced displacements. Among the infilled models, the concrete block infill resulted in the least displacement with a reduction of 80% compared to the bare frame, followed by clay brick infill which reduced the displacement by 73% as shown in Table 4-3 and 4-4. This trend was consistent in the 5-storey and 10-storey models as shown in Figures 4.8 and 4.9, where bare frames continued to show the highest displacement, and concrete block-infilled frames consistently outperformed the clay brick-infilled frames in minimising lateral displacement.

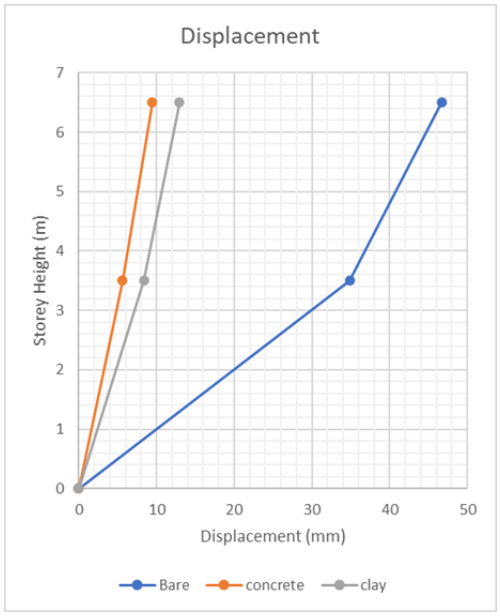

Figure 4.7 G+1 Storey Displacement

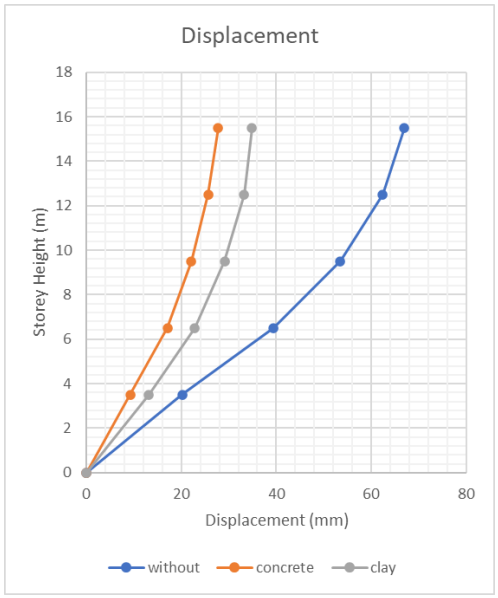

Figure 4.8 G+4 Storey Displacement

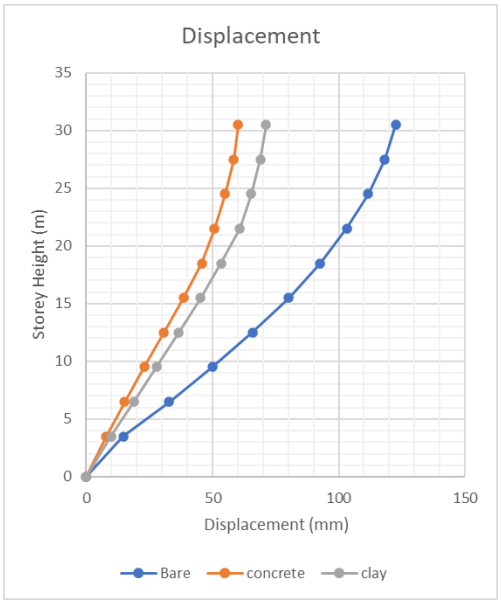

Figure 4.9 G+9 Storey Displacement

4.4.2 Storey Drift

As seen from Figure 4.10, storey drift is greatest for the bare frame, while the frames with infill have a smaller storey drift, with the concrete block infill having a smaller storey drift than the clay brick infill, with a Drift reduction of 84% and 77.6% respectively as shown in Table 4.3 and 4.4. It is also observed that all 3 cases have their highest storey drift at the first storey. The Trend of masonry infill reducing the storey drift is continued for the 5 and 10 storey structures, as shown in Figures 4.11 and 4.12. Notably, the soft-storey effect remained pronounced in all configurations, as the infills above acted as rigid diaphragms, forcing inelastic deformation to concentrate at the base. However, unlike the 2-storey structure, and the 5-storey structure, the 10-storey structure has a greater storey drift at the second storey instead of the first.

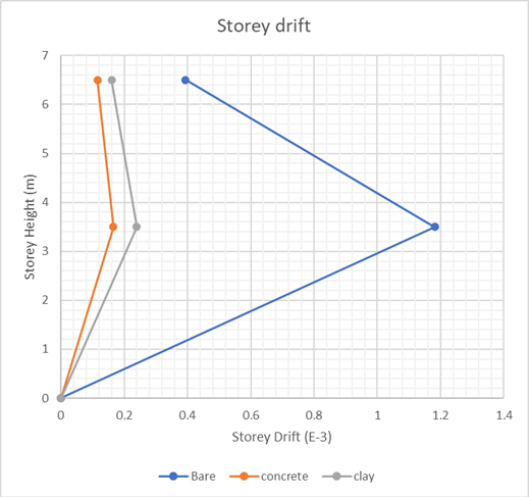

Figure 4.10 G+1 Storey Drift(%)

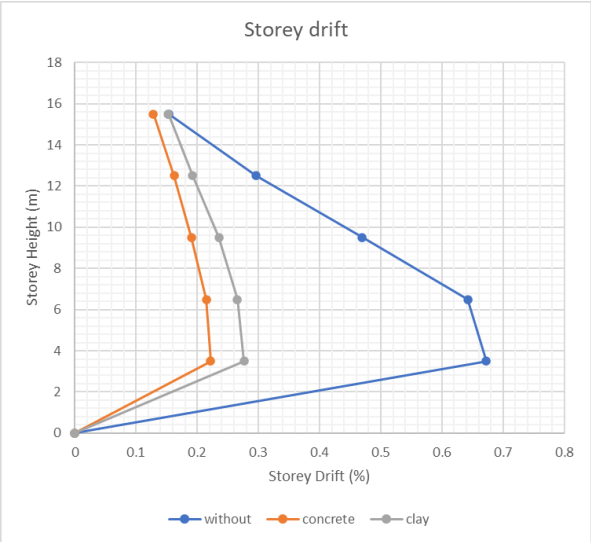

Figure 4.11 G+4 Storey Drift

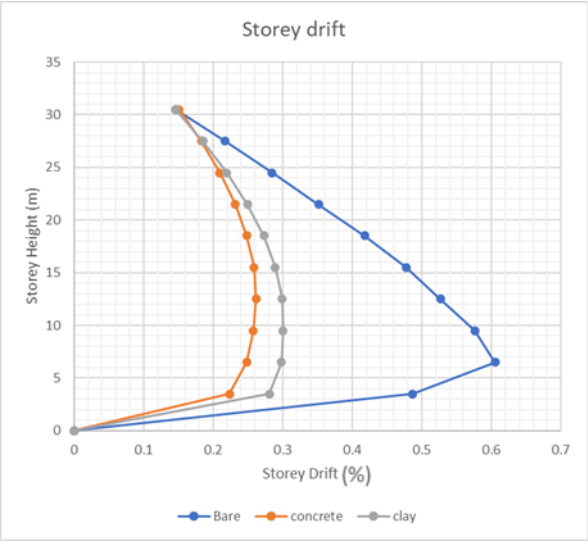

Figure 4.12 G+9 Storey Drift

4.4.3 Base shear

For the 2-storey structure as shown in Figure 4.13. The base shear for the frames with infill is observed to be larger than that of the bare frame. Among the infilled frames, those with concrete block infill exhibited higher base shear values than those with clay brick infill, with an increase of 689% and 664% respectively. This trend was also observed in the 5-storey and 10-storey structures, as seen in Figures 4.14 and 4.15. Across all cases, base shear was observed to be highest at the base and reduced progressively with height, forming a stair-step distribution pattern. This consistent behaviour across varying building heights indicates a clear influence of infill materials on the seismic response of the structure.

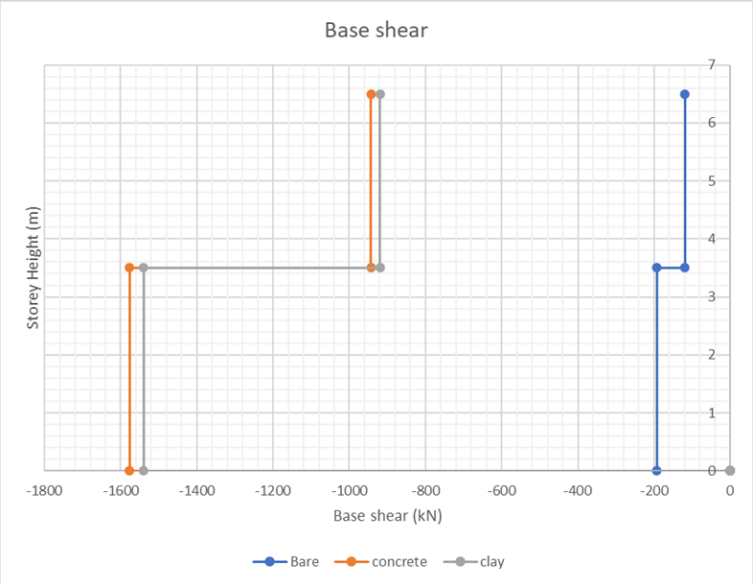

Figure 4.13 G+1 Base shear

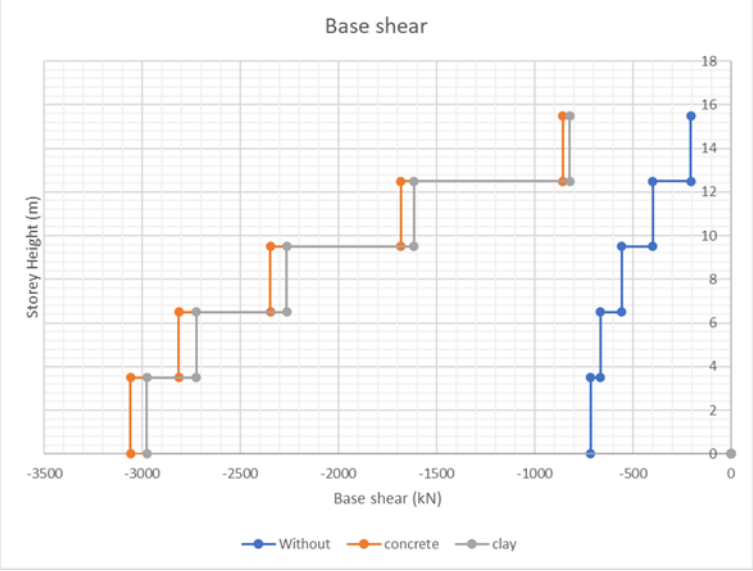

Figure 4.14 G+4 Base shear

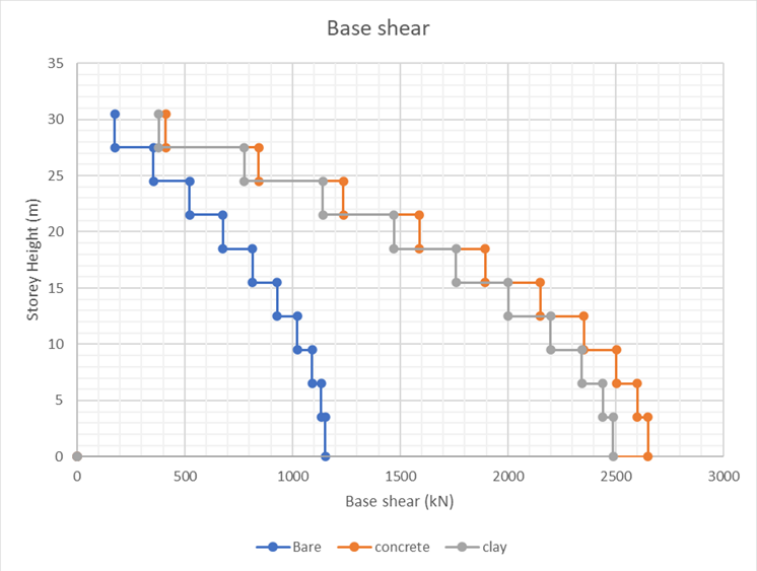

Figure 4.15 G+9 Base shear

4.4.4 Stiffness contribution

The analysis quantified the effect of masonry infill by calculating the percentage differences in maximum displacement, storey drift, and base shear for 2-, 5-, and 10-storey structures using both concrete block and clay brick infills. Results, as presented in Tables 4-3 and 4-4, show that neglecting infills in structural analysis leads to substantial overestimation of displacement and storey drift, by up to 79.7% and 84%, respectively, for 2-storey structures with concrete infill. Conversely, base shear was significantly underestimated by as much as 689%. Among the two types of infill, concrete block infills exhibited more pronounced effects than clay brick infills, due to their relatively higher stiffness and strength. Graphical representations shown in Figures 4.16 to 4.18 illustrate a decreasing trend in percentage differences with increasing number of storeys, indicating that the influence of infill walls diminishes with building height.

Table 4-3 Quantified effect of Concrete block infill on RC frame

Storey	**% Difference**		
	Displacement	Storey Drift	Base shear
G+1	79.7	84	689
G+4	59.8	67	330
G+9	50.9	59	130

Table 4-4 Quantified effect of Clay brick infill on RC Frame

Storey	% Difference		
	Displacement	Storey Drift	Base shear
G+1	73	77.6	664
G+4	48	59.7	318
G+9	42	50.7	116

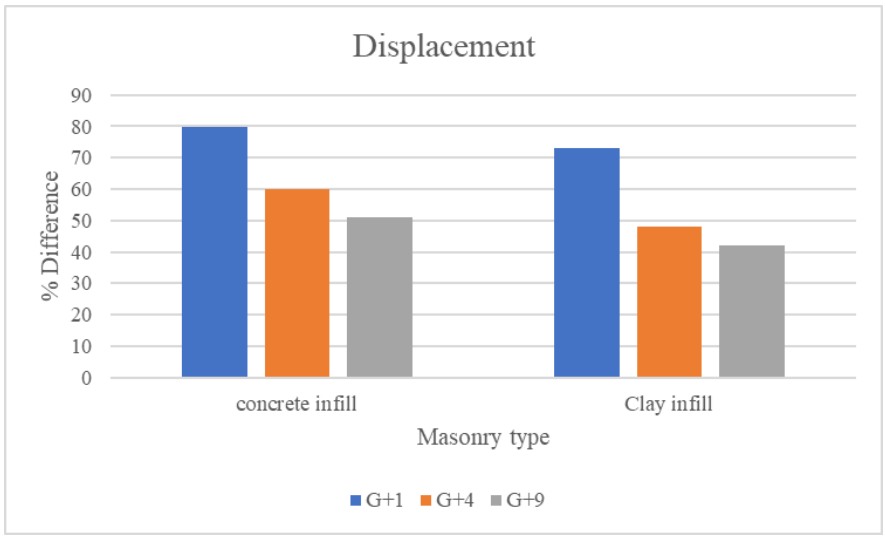

Figure 4.16 Percentage difference of Displacement at different heights

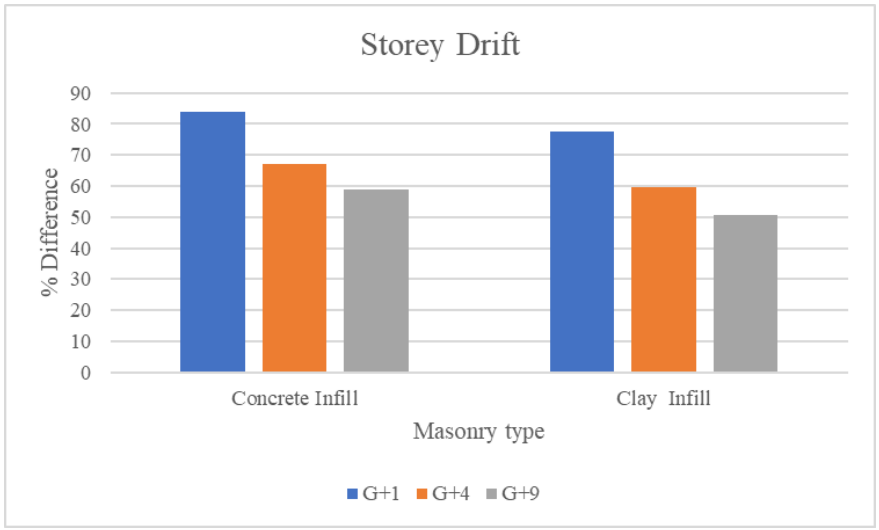

Figure 4.17 Percentage difference of Storey Drift at different heights

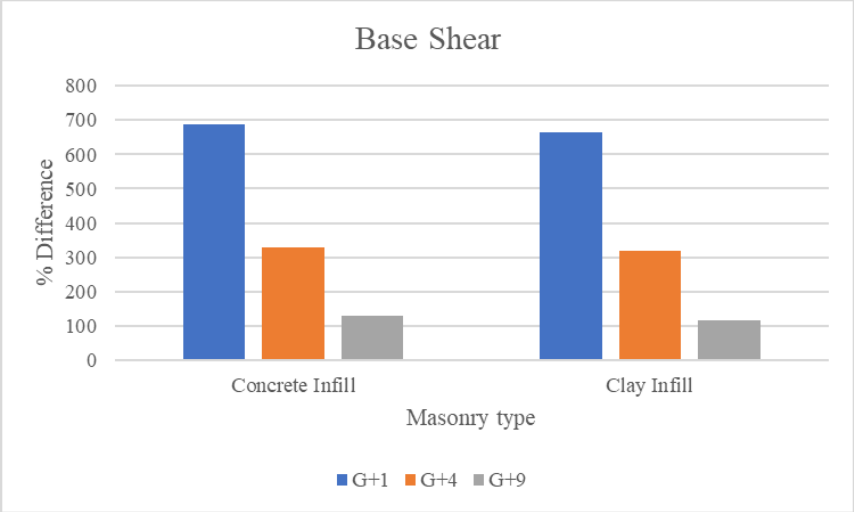

Figure 4.18 Percentage difference of base shear at different heights

CHAPTER 5: DISCUSSION

5.1 Design response spectrum

The developed site-specific design response spectrum for Fort Portal represents a significant advancement over the generalised spectra provided in the Uganda Seismic Code (US 319:2003). While the national code offers a uniform framework for seismic design across broad zoning categories, it does not fully capture Uganda's localised seismic hazard characteristics of highly active regions such as Fort Portal.

The developed spectrum for Fort Portal shows notably high spectral accelerations, especially in the short-to-medium period range (0.1–1.0s). This indicates that structural systems in this region are subjected to higher seismic demands than those predicted by the standard code provisions. Therefore, the Uganda Seismic Code generalised seismic zoning factors may underestimate site-specific effects. Consequently, adopting the developed spectrum ensures that critical parameters such as base shear, inter-storey drifts, and inelastic deformation demands are more realistically accounted for.

In practical terms, this means that designing structures using the developed Fort Portal spectrum results in higher design forces than the generalised spectra provided in the Uganda code. This aligns better with the actual seismic risk of the region and significantly reduces the probability of structural failure. However, caution is advised against the uneconomical use of the Fort Portal spectrum in lower seismic risk zones, such as zones 2 and 3, as it could lead to overdesign.

5.2 Discussion of FE model results

5.2.1 Bare RC frame

The pushover analysis of the bare RC frame, as simulated in Abaqus, revealed critical insights into the structural behaviour under lateral loading, particularly through the von Mises stress distribution. The von Mises stress served as an effective indicator of yielding and potential failure zones in both the concrete and masonry components (Dhir et al., 2021).

The maximum stress concentration at the beam-column joints, as observed in Figure 4.2, is due to the combined effects of bending moments, shear forces, and axial loads at these critical regions (Umwi & Alex, 2024). The stress values were seen to decrease progressively toward the mid-spans of beams and columns, indicating that the joints are the primary load-resisting elements under lateral loading. Moderate stresses are observed to appear in beam and column lengths, suggesting elastic behaviour with minor cracking, while low-stress regions dominate

areas farther from the joints, confirming their minimal role in resisting lateral loads (Yang et al., 2021).

5.2.2 RC frame with masonry infill

For the infilled RC frame, the diagonal stress patterns within the masonry, as shown in Figure 4.3, reflect a compressive strut action, where the infill behaves as a bracing element under lateral loading (Etemadi & Balkaya, 2024). This action resulted in the formation of principal stress bands extending diagonally from the top-loaded corner to the opposite base corner of the infill panel. This concentration shows how stress transfer occurs through diagonal compression struts within the masonry, while the RC frame resists flexural and shear demands (Sakr et al., 2017).

The corners along the direction of the diagonal strut were observed to remain in contact with the RC frame, while the opposite corners exhibited separation. This can be attributed to the compressive nature of the strut mechanism, which caused the infill to push against the top and bottom corners aligned with the applied lateral load (Nour et al., 2022). As the wall experiences compression along the strut path, these contact points are maintained and even intensified due to the force transmission. Conversely, the corners not along this path underwent tensile separation as the panel deformed and rotated slightly under load. Since masonry is weak in tension, cracking or detachment occurred in those zones (Borah et al., 2023).

5.3 Lateral strength versus drift relationships

From the graph in Figure 4.4, the RC frame with masonry infill is shown to exhibit a higher lateral force versus drift graph compared to that of the bare frame, which demonstrates that the infill enhanced the structural stiffness of the structure. The lateral force-drift graph plots the relationship between the applied horizontal force and the resulting drift of the structure. The steeper curve indicates greater resistance to deformation for a given force, meaning the structure is stiffer (Seki et al., 2018).

In the case of the infilled frame, the masonry infill acted as a rigid panel that interacts with the surrounding frame, effectively bracing it and distributing lateral loads more efficiently (Borah et al., 2023). This interaction reduced the overall lateral displacement under the same load compared to the bare frame, which relies solely on its own flexural and shear resistance (El-Kholy et al., 2024). The higher lateral force capacity at equivalent drift levels in the infilled frame confirms that the masonry infill contributes additional stiffness, restricting movement and improving the structure's overall rigidity. Thus, the elevated curve of the infilled frame directly reflects the stiffening effect of the masonry infill.

5.4 Validation and calibration of ETABS numerical models

The calibration process involved iterative modifications to the material properties, followed by successive analyses, to align the simulated outcomes of the storey displacements, inter-storey drifts, and base shear forces with the experimental results. By progressively fine-tuning the material parameters, the model achieved a close correlation with the physical test data, thereby enhancing its reliability for further structural assessments and design validations. This methodical calibration approach ensured that the analytical model effectively captured the nonlinear behaviour and load distribution observed in the experimental study.

5.5 Discussion of numerical model results

5.5.1 Displacement

The observed differences in displacement behaviour are primarily attributed to the additional stiffness provided by the infill walls. In the bare frame, lateral resistance was solely dependent on the beams, columns, and their joints, relying on their flexural and shear capacities (El-Kholy et al., 2024). The absence of infill walls resulted in a lack of supplemental lateral stiffness, leading to greater displacements under lateral loads. When infill was introduced, it acted like a braced system with the frame, increasing overall stiffness and reducing deformation (Khan et al., 2019).

This interaction is attributed to the diagonal strut action, where the infill helps distribute lateral forces more effectively. The degree of stiffness enhancement is observed to vary with the type of infill material. Concrete blocks, with a higher elastic modulus and compressive strength, provided a more rigid frame-infill interaction than clay bricks, explaining the lower displacements in the concrete block-infilled frames. In contrast, clay bricks, while still beneficial, are typically less stiff and more prone to early cracking, diminishing their capacity to resist deformation (Onat & Evci, 2024). As building height increased, the overall displacement was seen to grow due to increased global flexibility of the structure. However, the relative benefit of infill walls remained evident across all heights.

5.5.2 Storey Drift

For the bare frame, the lack of infill walls meant lateral resistance relied entirely on the flexural capacity of beams and columns, resulting in higher storey drifts, particularly at the ground level where seismic forces concentrate. This is because the base of the structure experiences the highest shear forces and moments, leading to more pronounced deformation at the lower levels (Etemadi & Balkaya, 2024).

The introduction of masonry infills significantly reduced drifts by providing additional stiffness through diagonal strut action, which distributed lateral loads more efficiently across the structure (Ramachandra et al., 2020). The difference in drift reduction between concrete block and clay brick infills stems from their distinct material properties. Concrete blocks typically have higher compressive strength and elastic modulus than clay bricks, creating stiffer infill panels that better resist shear deformation (Onat & Evci, 2024). This increased stiffness in concrete block-infilled frames led to smaller inter-storey drifts compared to clay brick-infilled frames. In taller buildings, such as the 10-storey structure, the shift in maximum drift to the second storey arose from higher-mode effects and interactions between the flexible lower frames and stiffer upper storeys (Kong et al., 2022).

5.5.3 Base shear

The results of the study revealed a significant increase in base shear for the reinforced concrete frames when masonry infill walls were incorporated. For the 2-, 5- and 10-storey buildings with concrete infill, the base shear increased by 689%, 330% and 130% respectively, when compared to the corresponding bare frame models. This trend is consistent with established seismic behaviour of infilled frames and can be explained by the substantial increase in global stiffness and added mass introduced by the masonry infill. When infill walls were introduced, they acted as diagonal struts that stiffened the structure, especially in the 2-storey structure where the infill occupied a large proportion of the structural height. The increased stiffness resulted in significantly shorter fundamental periods, which in turn shifted the structural response to a region of the design response spectrum associated with higher spectral accelerations. Since base shear is directly proportional to the spectral acceleration, this led to an increase in Base shear (Pudjisuryadi et al., 2021). This effect is particularly pronounced in the 2- and 5-storey buildings, whose initial periods lie near the steep descending branch of the response spectrum, where small period changes cause large changes in seismic demand.

The inclusion of infill walls, whether concrete blocks or clay bricks, also adds significant dead load to the system, thereby increasing the total seismic weight. This added mass results in higher inertial forces under seismic excitation, leading to greater base shear demands (El-Kholy et al., 2024). While both concrete blocks and clay bricks contribute to increased weight, concrete blocks typically generate higher base shear values due to their greater density and stiffness, which enhance both the mass and the structural rigidity of the system (Onat & Evci, 2024). Thus, the rise in base shear for infilled frames is a combined consequence of increased spectral acceleration and seismic weight (El-Kholy et al., 2024).

As the number of storeys increased, however, the relative contribution of each infill panel to the overall lateral stiffness decreased. In taller structures, the fundamental period is generally longer and lies in flatter portions of the spectrum where changes in stiffness lead to more moderate changes in spectral acceleration. This explains the progressively smaller increases in base shear for the 5-storey and 10-storey models. Therefore, Infill effects are most dramatic in low-rise frames and diminish with increasing building height.

Although masonry infill walls increase the dead load and consequently the total seismic weight of the structure, the resulting increase in base shear should be viewed as an increase in force demand rather than a reduction in seismic performance. The accompanying reduction in lateral displacement and storey drift indicates improved deformation control, which is critical for preventing structural damage and collapse under seismic loading.

5.6 Stiffness contribution

The observed stiffness contribution suggests that the structural response mechanisms vary with building height, thereby influencing the contribution of masonry infill. In low-rise buildings, such as the 2-storey frame model, the infill walls act as key lateral load-resisting elements. Their presence significantly stiffens the frame, resulting in reduced displacements and drifts, as well as increased base shear. However, as building height increased, like in the G+9, the relative contribution of infill walls became less dominant. This was attributed to the increasing global flexibility of the frame, which meant that global bending of the beams and columns governed the lateral deformation pattern. Under these conditions, the stiffness provided by infill walls at individual storeys becomes small relative to the cumulative flexural flexibility of the entire frame height, which causes bending deformations and higher-mode effects to govern the structural response. In such cases, the infill-frame interaction plays a secondary role (Christopoulos & Zhong, 2022). Furthermore, the cumulative mass of the taller buildings also outweighed the stiffness contribution of the infill, making its influence less significant in the overall response. This led to longer periods and greater dominance of frame flexibility in the taller structures (Zhang & Far, 2022).

CHAPTER 6: CONCLUSIONS AND RECOMMENDATIONS

6.1 CONCLUSION

This chapter summarizes the key findings of the thesis in response to the three research objectives that were set out in Chapter 1.

6.1.1 Objective 1: Development of a site-specific design response spectrum

This study successfully developed a site-specific design response spectrum for Fort Portal, located in Zone 1, the highest seismic risk area in Uganda. Using probabilistic seismic hazard assessment data from Oleng et al. (2024) and applying ASCE 7-22 procedures, the spectrum was tailored to the region's seismic characteristics, accounting for a peak ground acceleration of 0.255 g. The resulting curve, as shown in Figure 4.1, captured the local seismic hazard across all relevant periods, ensuring that structural designs based on it would be both location and hazard-specific. The developed Fort Portal design spectrum highlights that the national code underestimates seismic demand in the region and that site-specific spectra are critical for ensuring resilient infrastructure. Adoption of such refined spectra would represent a step towards performance-based seismic design in Uganda, bridging the gap between simplified code provisions and actual seismic hazard realities. This spectrum provides engineers with a reliable baseline for performance-based seismic design in Uganda's most hazardous seismic zone, reducing reliance on generic code provisions.

6.1.2 Objective 2: Development of representative numerical models of Reinforced Concrete frames with and without masonry infills

Finite Element micromodelling in ABAQUS and equivalent diagonal strut macromodelling in ETABS were used to create numerical models that accurately represent the in-plane behaviour of RC frames with and without masonry infill. Model validation was carried out using published experimental data from pseudo-dynamic tests, with both approaches achieving close agreement in displacement, drift, and base shear trends. The validated ABAQUS model provided a detailed reference for local stress distribution, while the ETABS diagonal strut models proved computationally efficient for multi-storey analyses. Final numerical models were developed for G+1, G+4, and G+9 storey buildings using both clay brick and solid concrete block infills, enabling consistent and scalable simulations.

6.1.3 Objective 3: Determination of the seismic response of the numerical models under seismic loading by carrying out a pushover analysis

Nonlinear static pushover analyses revealed that masonry infill walls significantly enhance the seismic performance of RC frames, with the extent of improvement influenced by infill material type and building height. Solid concrete block infills provided the highest initial stiffness and base shear capacity, followed by clay brick infills. Both infill types reduced roof displacement and storey drift and increased Base shear compared to bare frames, with more pronounced benefits in low and mid-rise structures. Displacement was reduced by 79.7% for the concrete infill in the 2-storey structure and by 73 % for the clay infill, and Base shear was increased by 689% and 664% respectively, as shown in Tables 4-3 and 4-4. The concurrent reduction in lateral displacement and storey drift alongside an increase in base shear indicates that the presence of masonry infill walls leads to a stiffer structural system that attracts higher seismic forces but resists them with improved deformation control.

However, the stiffness contribution decreased as building height increased. This is observed by concrete infill reducing displacement by 80% in the 2-storey structure, but reducing it by 50% in the 10-storey structure. This diminishing relative influence in taller frames is due to the greater flexibility of taller structures and the reduced interaction between infill and frame. This finding suggests that while infill walls can be highly beneficial for low-rise construction in Uganda, their seismic contribution must be carefully evaluated in taller buildings to avoid over-reliance on their stiffness, which may lead to unintended shear failures or torsion effects.

6.2 RECOMMENDATIONS

6.2.1 Practical recommendations

Current seismic design guidelines in Uganda should explicitly account for the stiffness and strength contributions of masonry infill walls, particularly for low- and mid-rise buildings. Since infills significantly reduce displacements and drifts while increasing base shear, their presence must be incorporated into structural modelling and load calculations to avoid underestimating lateral demands or overestimating ductility. Designers should therefore account for infill frame interaction by adopting the equivalent diagonal strut method using Mainstone's equation.

The increased stiffness and mass introduced by infills result in higher base shear demands, which must be adequately accounted for through proper shear design and detailing of structural elements. Ensuring sufficient shear capacity allows designers to fully benefit from the positive effects of infill walls while avoiding brittle failure mechanisms.

Although masonry infill walls significantly enhance the seismic performance of low-rise reinforced concrete buildings by providing additional stiffness and reducing lateral displacements, their relative contribution diminishes as building height increases. Therefore, engineers should adopt alternative or supplementary structural systems, such as reinforced concrete shear walls, steel bracing systems, or core wall systems, to ensure adequate stiffness, strength, and ductility in taller buildings.

6.2.2 Future academic research

While the current work focused on clay bricks and solid concrete blocks, other locally prevalent materials, such as stabilized soil blocks and other types of structural frames, are also used in construction and may exhibit different seismic responses. Conducting systematic laboratory experiments on these materials, combined with numerical simulations across different structural configurations, would provide a more comprehensive understanding of how infill typologies influence seismic performance.

Although this study employed nonlinear static pushover analysis to evaluate the seismic performance of the models, Future research should adopt non-linear time history analysis where feasible, as it provides a more realistic representation of structural response under seismic loading by capturing actual ground motion characteristics. This should be used to calibrate and validate the simplified pushover methods for the specific frame and infill types studied.

Future research should also focus on understanding how the irregular distribution of infill walls and the presence of soft-storey mechanisms influence the seismic performance of reinforced concrete buildings in Uganda. This can shed light on the potential hazards that arise when infills are unevenly distributed or absent at certain levels, particularly the ground storey.

REFERENCES

Ackomah, H. G., Mensah, Lord, & Kuttu, S. (2024). Natural disaster and Economic Growth in Africa: The role of Insurance. *Cogent Economics and Finance*, *12*(1). https://doi.org/10.1080/23322039.2024.2328480

Ahiwale, D. D., Khartode, R. R., & Raut, K. V. (2020). Seismic Response for RC Frames on Sloping Ground using Pushover Analysis. *Journal of Structural Engineering and Management*, *7*(2), 36–46. www.stmjournals.com

Akinradewo, O. F., & Adedokun, D. O. (2020). Comparative Cost Analysis of using Conventional Blocks and Interlocking Bricks for Mass Housing in Nigeria. *Covenant Journal of Research in the Built Environment*, *8*(1). https://doi.org/10.47231/wxgy9716

Al-hagri, M. G., Nakipoglu, A., & Döndüren, M. S. (2023). Effect of Arrangement of Masonry Infill walls, Shear Walls and Steel Bracings on the Story Drift and Stiffness Irregularity. *Advanced Engineering Science*, *3*, 85–97.

Arêde, A., Almeida, C., Costa, C., & Costa, A. (2019). In-Situ and lab Tests for Mechanical Characterization of Stone Masonry Historical Structures. *Construction and Building Materials*, *220*, 503–515. https://doi.org/10.1016/j.conbuildmat.2019.06.039

ASCE. (2022). Minimum Design Loads and Associated Criteria for Buildings and Other Structures (ASCE/SEI 7-22). In *Minimum Design Loads and Associated Criteria for Buildings and Other Structures*. https://doi.org/10.1061/9780784415788.sup3

Ashwini, K., Keshavamurthy, M., & Ravikumar, C. M. (2024). Pushover Analysis a Review. *Journal of Emerging Technologies and Innovative Research*, *11*(2).

Bagnoli, M., Grande, E., & Milani, G. (2022). Reinforced Concrete Infilled Frames. *Encyclopedia*, *2*(1), 473–485. https://doi.org/10.3390/encyclopedia2010030

Bantidi, T. M. (2023). Effect of Permanent Stress on the Time-Dependent Earthquake Probability: Implication for Seismic Hazard Assessment in the African Continent. *Geophysical Journal International*, *234*(2), 1073–1091. https://doi.org/10.1093/gji/ggad121

Bilgin, H., & Plaku, B. (2024). Influence of Confined Concrete Models on the Seismic Response of RC Frames. *Structural Durability & Strength Monitoring*. https://doi.org/10.32604/sdhm.2024.048645

Borah, B., Kaushik, H. B., & Singhal, V. (2023). Analysis and Design of Confined Masonry Structures: Review and Future Research Directions. *Buildings*, *13*(5).

https://doi.org/10.3390/buildings13051282

Chen, P.-C., & Chen, P.-C. (2023). Real-Time Hybrid Simulation for Seismic Control Performance Evaluation of an Active Inerter Damper System. *Engineering Structures*, *294*. https://doi.org/10.1016/j.engstruct.2023.116760

Cheriberi, D., & Yee, E. (2022). Preliminary Seismic Hazard Analyses for the Ugandan Region. *Applied Sciences (Switzerland)*, *12*(2). https://doi.org/10.3390/app12020598

Christopoulos, C., & Zhong, C. (2022). Towards understanding, estimating and mitigating higher-mode effects for more resilient tall buildings. *Resilient Cities and Structures*, *1*(1), 53–64. https://doi.org/10.1016/j.rcns.2022.03.005

Delforge, D., Wathelet, V., Below, R., Sofia, C. L., Tonnelier, M., van Loenhout, J. A. F., & Speybroeck, N. (2025). EM-DAT: the Emergency Events Database. *International Journal of Disaster Risk Reduction*, *124*. https://doi.org/10.1016/j.ijdrr.2025.105509

Dhir, P. K., Tubaldi, E., Ahmadi, H., & Gough, J. (2021). Numerical Modelling of Reinforced Concrete Frames with Masonry Inflls and Rubber Joints. *Engineering Structures*, *246*(8). https://doi.org/10.1016/j.engstruct.2021.112833

Di Trapani, F., Macaluso, G., Cavaleri, L., & Papia, M. (2014). Masonry infills and RC frames interaction: Literature overview and state of the art of macromodeling approach. *European Journal of Environmental and Civil Engineering*, *19*(9), 1059–1095. https://doi.org/10.1080/19648189.2014.996671

Dias-Oliveira, J., Rodrigues, H., Asteris, P. G., & Varum, H. (2022). On the Seismic Behavior of Masonry Infilled Frame Structures. *Buildings*, *12*(8). https://doi.org/10.3390/buildings12081146

El-Kholy, A. M., Sayed, S. M., & El-Assaly, M. M. (2024). Nonlinear Macromodeling of Multistory RC Buildings with Masonry Infill Walls. In *Bulletin of Earthquake Engineering* (Vol. 22, Issue 3). Springer Netherlands. https://doi.org/10.1007/s10518-023-01787-8

Etemadi, A., & Balkaya, C. (2024). The Role of Masonry Infills on the Interstory Drift Demand of Reinforced Concrete Frames. *Soil Dynamics and Earthquake Engineering*, *180*(March 2023). https://doi.org/10.1016/j.soildyn.2024.108599

FEMA P-58. (2018). Seismic Performance Assessment of Buildings. *NCEE 2014 - 10th U.S. National Conference on Earthquake Engineering: Frontiers of Earthquake Engineering*, *1*(December). https://doi.org/10.4231/D3ZW18S8N

Guettala, S., Abdesselam, I., & Chebili, R. (2023). Seismic Performance and Numerical Modeling of Masonry Infill Walls : A Comprehensive Overview. *1st International Conference on Civil and Earthquake Engineering*.

Holmes, M. (1961). Steel Frames with Brickwork and Concrete Infilling. *Proceedings of the Institution of Civil Engineers*.

Hori, Y., Suzuki, Y., Kolozvari, K., Johansson, O., Naeim, F., & Nakashima, M. (2022). A comparative study of seismic analysis, design, and collapse safety margins of tall buildings in the United States and Japan, Part I: Performance-based analysis and design. *Earthquake Spectra*, *38*(3), 2297–2318. https://doi.org/10.1177/87552930221076528

Islam, T., & Sen, D. (2023). Numerical modelling and validation of lateral behavior of masonry-infilled RC frame focusing sliding failure of infill panel. *Asian Journal of Civil Engineering*, *24*(5), 1247–1255. https://doi.org/10.1007/s42107-022-00566-1

Khan, N. A., Tahir, M. F., Nuti, C., Briseghella, B., & Bergami, A. V. (2019). Influence of brick masonry infill walls on seismic response of RC structures. *Technical Journal, UET Taxila*, *24*(3), 15–23.

Khiatine, M., Medjnoun, A., Aiche, O., & Bahar, R. (2025). Nonlinear ground performance under a high shaking scenario similar to Boumerdes earthquake. *Materials Research Proceedings*, *48*, 242–251. https://doi.org/10.21741/9781644903414-27

Khokhar, R., & Brzev, S. (2021). Simplified criteria for the prediction of shear failure mechanism in low-rise RC frames with masonry infills. *Asian Journal of Civil Engineering*. https://doi.org/10.1007/s42107-021-00393-w

Kia, M., Amini, A., Bayat, M., & Ziehl, P. (2021). Probabilistic Seismic Demand Analysis of Structures Using Reliability Approaches. *Journal of Earthquake and Tsunami*, *15*. https://doi.org/10.1142/S1793431121500111

Kong, J., Su, Y., Zheng, Z., Wang, X., & Zhang, Y. (2022). The Influence of Vertical Arrangement and Masonry Material of Infill Walls on the Seismic Performance of RC Frames. *Buildings*, *12*(6). https://doi.org/10.3390/buildings12060825

Lakshani, M. M. T., Jayathilaka, T. K. G. A., & Thamboo, J. A. (2020). Experimental investigation of the unconfined compressive strength characteristics of masonry mortars. *Journal of Building Engineering*, *32*(June). https://doi.org/10.1016/j.jobe.2020.101558

Mainstone, R. J. (1971). On the stiffnesses and strengths of infilled frames. *7360 S*, 34.

Mandal, A. (2023). What is pushover analysis and how to perform it in ETABS? *Structure*

Realm. https://civilengineering-mcq.web.app/structural-engineering/What-is-pushover-analysis-and-how-to-perform-it-in-ETABS

Milijaš, A., Marinković, M., Butenweg, C., & Klinkel, S. (2024). Experimental investigation on the seismic performance of reinforced concrete frames with decoupled masonry infills: considering in-plane and out-of-plane load interaction effects. In *Bulletin of Earthquake Engineering* (Vol. 22, Issue 15). Springer Netherlands. https://doi.org/10.1007/s10518-024-02012-w

Morandi, P., Hak, S., & Magenes, G. (2017). Experimental and numerical seismic performance of strong clay masonry infills. In appendix: guideline proposal for seismic design of masonry infills. *Eucentre*, *September*, 214.

Morandi, P., Hak, S., Milanesi, R. R., & Magenes, G. (2021). In-plane/out-of-plane interaction of strong masonry infills:From cyclic tests to out-of-plane verifications. *Earthquake Engineering & Structural Dynamics*. https://doi.org/10.1002/eqe.3584

Moreira, R. F., Varum, H., & Castro, J. M. (2023). Influence of Masonry Infill Walls on the Seismic Assessment of Non-Seismically Designed RC Framed Structures. *Buildings*, *13*(5), 1–34. https://doi.org/10.3390/buildings13051148

Mucedero, G., Perrone, D., & Monteiro, R. (2022). Epistemic uncertainty in poorly detailed existing frames accounting for masonry infill variability and RC shear failure. *Earthquake Engineering & Structural Dynamics*. https://doi.org/10.1002/eqe.3748

Negro, P., & Verzeletti, G. (1996). Effect on infills on the global behaviour of R/C frames: energy considerations from pseudodynamic tests. *Earthquake Engineering and Structural Dynamics*, *25*(8), 753–773.

Nour, A., Benanane, A., & Varum, H. (2022). Importance of Infill Masonry Walls in Improving the Seismic Response of Reinforced Concrete Buildings. *International Journal on Advanced Science, Engineering and Information Technology*, *12*(2), 642–648. https://doi.org/10.18517/ijaseit.12.2.14040

Nour, A., Bourdim, S. M. E. A., & Terki Hassaine, M. I. E. (2023). Evaluation of the Seismic Behavior of RC Buildings through the Direct Modeling of Masonry Infill Walls. *Buildings*, *13*(7). https://doi.org/10.3390/buildings13071576

Oleng, M., Ozdemir, Z., & Pilakoutas, K. (2024). Probabilistic seismic hazard assessment framework for Uganda : a stochastic event - based modelling approach. In *Bulletin of Earthquake Engineering* (Vol. 22, Issue 4). Springer Netherlands. https://doi.org/10.1007/s10518-024-01856-6

Onat, Ö., & Evci, P. U. (2024). A parametric study in reinforced concrete frames with different infill wall materials. *Bulletin of Earthquake Engineering*, *22*(9), 4447–4476. https://doi.org/10.1007/s10518-024-01936-7

Pallarés, F. J., Davia, A., Hassan, W. M., & Pallarés, L. (2021). Experimental and Analytical Assessment of the Influence of Masonry Façade Infills on Seismic Behavior of RC Frame Buildings. *Engineering Structures*, *235*(6), 1–20. https://doi.org/10.1016/j.engstruct.2021.112031

Petreski, B., & Gjorgjiev, I. (2021). Residual Drift Estimation for Moment Resisting Frames with Steel Degradation Properties. *Ce/Papers*, *4*(2–4), 1917–1923. https://doi.org/10.1002/cepa.1504

Pudjisuryadi, P., Prayogo, V. S., Oetomo, S. I., & Lumantarna, B. (2021). Seismic Performance of a Three-Story Reinforced Concrete Building with Masonry Infill Walls and Friction Base Support. *Civil Engineering Dimension*, *23*(1), 35–43. https://doi.org/10.9744/ced.23.1.35-43

Ramachandra, S., Ramakrishna, V. B., Vasantha, & Vedant, V. (2020). The Influence of Infill Masonry Wall in RC Frames Subjected to Seismic Load for Sustainable Structure. *IOP Conference Series: Materials Science and Engineering*, *955*(1). https://doi.org/10.1088/1757-899X/955/1/012024

Robert Meli, E. a. (2011). Seismic Design Guide for Low-Rise Confined Masonry Buildings. *World Housing*, *August*.

Roudane, B. (2019). Numerical Modeling of Masonry Infilled Reinforced Concrete Building during Construction Stages Using. *Buildings*, *9*(8). https://doi.org/10.3390/buildings9080181

Sakr, M., El-khoriby, S. R., Seleemah, A. A., & Darwish, E. A. (2017). FE Modeling of CFRP-Retrofitted RC Frames with Masonry Infill Walls. *Civil Engineering Journal*, *3*(4), 267–287. https://doi.org/10.28991/cej-2017-00000090

Seki, M., Popa, V., Lozinca, E., Dutu, A., & Papurcu, A. (2018). Experimental study on retrofit technologies for RC frames with infilled brick masonry walls in developing countries. *The 16th European Conference on Earthquake Engineering*, *June*, 1–12.

Sen, D., & Chowdhury, S. R. (2024). Finite Element Analysis on The Effect of Gap Between Masonry Infill and Reinforced Concrete Frame Under Inplane Loading. *Civil Engineering Infrastructures Journal*, *December*. https://doi.org/10.22059/ceij.2024.375383.2055

Stojadinović, Z., Kovačević, M., Marinković, D., & Stojadinović, B. (2022). Rapid earthquake loss assessment based on machine learning and representative sampling. *Earthquake Spectra*, *38*(1), 152–177. https://doi.org/10.1177/87552930211042393

Thaickavil, N. N., & Thomas, J. (2018). Behaviour and strength assessment of masonry prisms. *Case Studies in Construction Materials*, *8*, 23–38. https://doi.org/10.1016/j.cscm.2017.12.007

Toufik, M. A., & Salah, A. (2024). Evaluation of the Seismic Demand of Asymmetrical Buildings by the Adaptive Modal Pushover Procedure. *1st International Conference on Civil and Earthquake Engineering ICCEE2023*, *January*.

Umar, M., Shah, S. A. A., Shahzada, K., Naqash, T., & Ali, W. (2020). Assessment of seismic capacity for reinforced concrete frames with perforated unreinforced brick masonry infill wall. *Civil Engineering Journal (Iran)*, *6*(12), 2397–2415. https://doi.org/10.28991/cej-2020-03091625

Umwi, D., & Alex, J. (2024). Seismic Performance Assessment of Reinforced Concrete Frames: Insights from Pushover Analysis. *Proceedings of SECON'24*. https://doi.org/10.1007/978-3-031-70431-4_72

UNBC. (2019). The National Building (Structural Design) code. *Satutory Instruments Suppliment*, *CXI*.

UNBS. (2003). US 319 : 2003 UGANDA STANDARD Seismic code of practice for structural designs. *UNBS*, *June*, 2–26. https://webstore.unbs.go.ug//store.php?src=1701&preview

USGS. (2023). *Earthquake Hazard Program*. https://www.usgs.gov/programs/earthquake-hazards

Vijayan, D. S., Mohan, A., Revathy, J., Parthiban, D., & Varatharajan, R. (2021). Evaluation of the impact of thermal performance on various building bricks and blocks: A review. *Environmental Technology & Innovation*, *23*. https://doi.org/10.1016/j.eti.2021.101577

Wadembere, I., & Kobugabe, M. (2017). Geospatial Assessment of Uncontrolled Urbanization and Its Deviation from an Intelligent City : A Case Study of Fort Portal , Uganda. *Journal of Geography Environment and Earth Science International*, *October 2017*. https://doi.org/10.9734/JGEESI/2017/36362

Xie, X., Qu, Z., Fu, H., & Zhang, L. (2021). Effect of prior in-plane damage on the out-of-plane behavior of masonry infill walls. *Engineering Structures*, *226*, 1–18. https://doi.org/10.1016/j.engstruct.2020.111380

Xie, X., Zhang, L., & Qu, Z. (2020). A Critical Review of Methods for Determining the Damage States for the In-plane Fragility of Masonry Infill Walls. *Journal of Earthquake Engineering*. https://doi.org/10.1080/13632469.2020.1835749

Yang, T., Li, Y., & Zhai, X. (2021). Seismic performance analysis of reinforced concrete frame structures based on computational mechanics. *European Journal of Computational Mechanics*, *30*(1), 99–120. https://doi.org/10.13052/ejcm1779-7179.3014

Zhang, X., & Far, H. (2022). Seismic behaviour of high-rise frame-core tube structures considering dynamic soil–structure interaction. *Bulletin of Earthquake Engineering*, *20*(10), 5073–5105. https://doi.org/10.1007/s10518-022-01398-9

Zine, A., Kadid, A., & Zatar, A. (2021). Effect of masonry infill panels on the seismic response of reinforced concrete frame structures. *Civil Engineering Journal (Iran)*, *7*(11), 1853–1867. https://doi.org/10.28991/cej-2021-03091764

APPENDICES

APPENDIX I: Experimental Results

Table A-0-1 Properties of Concrete Block Samples

Dimensions (mm)	Weight (kg)	Crushing Force (kN)	SArea (mm^2)	Compressive strength (Mpa)
390x150x185	14.75	230	390x150	3.93
400x150x180	16.55	230	400x150	3.83
390x150x190	14.65	190	390x150	3.25
390x150x185	15.93	181	390x150	3.09
390x150x185	15.43	190	390x150	3.25
Mean				3.47

Table A-0-2 Properties of Clay Brick Samples

Dimensions (mm)	Weight (kg)	Crushing Force (kN)	SArea (mm^2)	Compressive strength (Mpa)
230x100x110	4.365	67	230x100	2.91
200x90x100	3.3	44	200x100	2.2
210x90x110	3.455	64	210x110	2.77
200x90x110	3.365	45	200x110	2.045
210x95x110	4.330	67	210x110	2.9
Mean				2.565

Table A-0-3 Mortar compressive strength for different mortar mixes

Mortar Designation	Type of mortar in volumetric proportions			Mean compressive strength at 28 days	
	Cement/ lime/sand	Cement/ sand	Cement/ sand with plasticizer	Preliminary lab tests (N/mm^2)	Tests from site samples (N/mm^2)
1	1:1/4:3	-	-	16.0	11.0
2	1:1/2:4	1:3	$1:3^1/_2$	6.5	4.5
3	$1:1:5^1/_2$	$1:4^1/_2$	$1:5^1/_2$	3.6	2.5
4	$1:2:8^1/_2$	1:6	$1:7^1/_2$	1.5	1.0

APPENDIX II: Diagonal strut Widths

Single Frame

f_m (MPa)	11.6
E_m (Mpa)	6380
Column CS (mm)	250
	250
Beam CS (mm)	250
	300
Height (mm)	2100
c-c (mm)	2250
L (mm)	2000
H (mm)	1800
Theta (^{0})	41.9872125
fc (Mpa)	25
Ec (Mpa)	25000
t (mm)	112
Ic	325520833.3
Gamma	0.001866145
alpha	3.359060605
Width (mm)	290.0148231

Four-storey Validation model strut widths (mm)

Storey Height \ **Beam span**	**4m**	**5m**	**6m**
3.5m	589.71076	694.558	809.8836
3m	584.4101	704.1868	833.5575

Numerical Models

Two-storey structure-Concrete masonry infill

Storey Height \ Beam span	4m	5m	6m
3.5m	464.9111	546.7295	635.9486
3m	463.2069451	556.2635	656.079

Two-storey structure-Clay masonry infill

Storey Height \ Beam span	4m	5m	6m
3.5m	489.7504	563.9522	665.9261
3m	487.9551	585.9835	691.132

Five-storey structure-Concrete masonry infill

Storey Height \ Beam span	4m	5m	6m
3.5m	537.7748556	632.9286	737.1239
3m	534.4003006	642.8569	759.5808

Five-storey structure-Clay masonry infill

Storey Height \ Beam span	4m	5m	6m
3.5m	566.5071	652.8668	776.5069
3m	562.9522	677.2034	800.1636

Ten-storey structure-Concrete masonry infill

Storey Height \ Beam span	4m	5m	6m
3.5m	593.4150433	698.9208	814.9709
3m	588.0811122	708.6102	838.7935

Ten-storey structure-Clay masonry infill

Storey Height \ Beam span	4m	5m	6m
3.5m	625.12	694.558	858.5131
3m	619.5011	746.4697	883.6085

APPENDIX III: Fort portal Design Spectrum Coordinates

Period T (s)	Sa/g	Period T (s)	Sa/g	Period T (s)	Sa/g	Period T (s)	Sa/g	Period T (s)	Sa/g	Period T (s)	Sa/g
0.000	0.433	1.834	0.138	3.534	0.072	5.234	0.048	6.934	0.037	8.600	0.027
0.047	1.083	1.884	0.134	3.584	0.071	5.284	0.048	6.984	0.036	8.650	0.027
0.234	1.083	1.934	0.131	3.634	0.070	5.334	0.047	7.034	0.036	8.700	0.027
0.284	0.893	1.984	0.128	3.684	0.069	5.384	0.047	7.084	0.036	8.750	0.026
0.334	0.759	2.034	0.125	3.734	0.068	5.434	0.047	7.134	0.036	8.800	0.026
0.384	0.660	2.084	0.122	3.784	0.067	5.484	0.046	7.184	0.035	8.850	0.026
0.434	0.584	2.134	0.119	3.834	0.066	5.534	0.046	7.234	0.035	8.900	0.026
0.484	0.524	2.184	0.116	3.884	0.065	5.584	0.045	7.284	0.035	8.950	0.025
0.534	0.475	2.234	0.113	3.934	0.064	5.634	0.045	7.334	0.035	9.000	0.025
0.584	0.434	2.284	0.111	3.984	0.064	5.684	0.045	7.384	0.034	9.050	0.025
0.634	0.400	2.334	0.109	4.034	0.063	5.734	0.044	7.434	0.034	9.100	0.024
0.684	0.370	2.384	0.106	4.084	0.062	5.784	0.044	7.484	0.034	9.150	0.024
0.734	0.345	2.434	0.104	4.134	0.061	5.834	0.043	7.534	0.034	9.200	0.024
0.784	0.323	2.484	0.102	4.184	0.061	5.884	0.043	7.584	0.033	9.250	0.024
0.834	0.304	2.534	0.100	4.234	0.060	5.934	0.043	7.634	0.033	9.300	0.023
0.884	0.287	2.584	0.098	4.284	0.059	5.984	0.042	7.684	0.033	9.350	0.023
0.934	0.271	2.634	0.096	4.334	0.058	6.034	0.042	7.734	0.033	9.400	0.023
0.984	0.257	2.684	0.094	4.384	0.058	6.084	0.042	7.784	0.033	9.450	0.023
1.034	0.245	2.734	0.093	4.434	0.057	6.134	0.041	7.834	0.032	9.500	0.022
1.084	0.234	2.784	0.091	4.484	0.056	6.184	0.041	7.884	0.032	9.550	0.022
1.134	0.223	2.834	0.089	4.534	0.056	6.234	0.041	7.934	0.032	9.600	0.022
1.184	0.214	2.884	0.088	4.584	0.055	6.284	0.040	7.984	0.032	9.650	0.022
1.234	0.205	2.934	0.086	4.634	0.055	6.334	0.040	8.000	0.032	9.700	0.022
1.284	0.197	2.984	0.085	4.684	0.054	6.384	0.040	8.050	0.031	9.750	0.021

1.334	0.190	3.034	0.084	4.734	0.054	6.434	0.039	8.100	0.031	9.800	0.021
1.384	0.183	3.084	0.082	4.784	0.053	6.484	0.039	8.150	0.031	9.850	0.021
1.434	0.177	3.134	0.081	4.834	0.052	6.534	0.039	8.200	0.030	9.900	0.021
1.484	0.171	3.184	0.080	4.884	0.052	6.584	0.038	8.250	0.030	9.950	0.020
1.534	0.165	3.234	0.078	4.934	0.051	6.634	0.038	8.300	0.029	10.000	0.020
1.584	0.160	3.284	0.077	4.984	0.051	6.684	0.038	8.350	0.029		
1.634	0.155	3.334	0.076	5.034	0.050	6.734	0.038	8.400	0.029		
1.684	0.150	3.384	0.075	5.084	0.050	6.784	0.037	8.450	0.028		
1.734	0.146	3.434	0.074	5.134	0.049	6.834	0.037	8.500	0.028		
1.784	0.142	3.484	0.073	5.184	0.049	6.884	0.037	8.550	0.028		

APPENDIX IV: Representative numerical models from ETABS

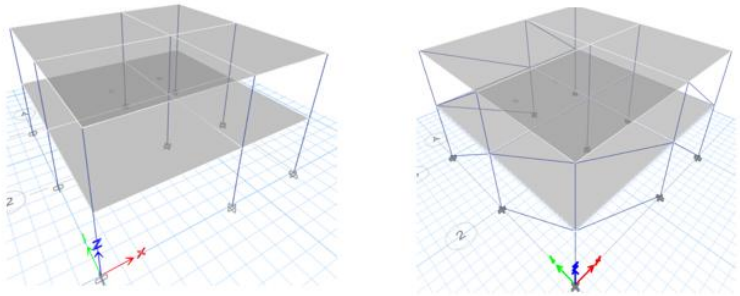

Figure A.0.1 Two-storey models, with and without infill

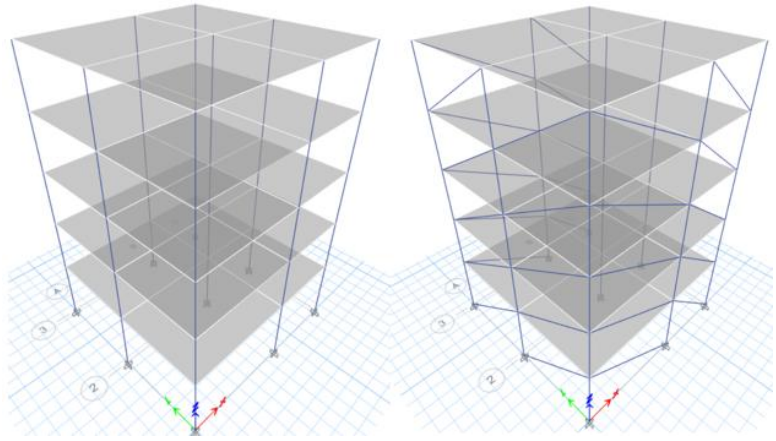

Figure A.0.2 Five-storey models, with and without infill

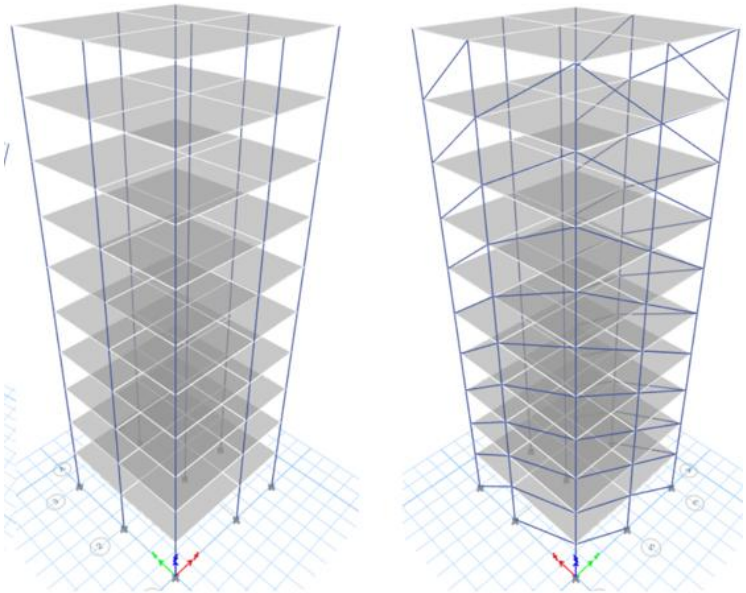

Figure A.0.3 Ten-storey models, with and without infill